

Influence of Embedded HVDC Transmission on AC Network Performance

by

Jicheng Yu

A Thesis Presented in Partial Fulfillment
of the Requirements for the Degree
Master of Science

Approved November 2013 by the
Graduate Supervisory Committee:

George Karady, Chair
Yu Hui
Keith Holbert

ARIZONA STATE UNIVERSITY

December 2013

ABSTRACT

An embedded HVDC system is a dc link with at least two ends being physically connected within a single synchronous ac network. The thesis reviews previous works on embedded HVDC, proposes a dynamic embedded HVDC model by PSCAD program, and compares the transient stability performance among AC, DC and embedded HVDC. The test results indicate that by installing the embedded HVDC, AC network transient stability performance has been largely improved. Therefore the thesis designs a novel frequency control topology for embedded HVDC. According to the dynamic performance test results, when the embedded HVDC system equipped with a frequency control, the system transient stability will be improved further.

TABLE OF CONTENTS

	Page
CHAPTER	
1 BACKGROUND INFORMATION AND LITERATURE REVIEW	1
1.1 State of the art	2
1.2 Existing embedded HVDC description	21
2 SYSTEM TECHNICAL PERFORMANCE ISSUES WITH EMBEDDED HVDC LINKS	34
2.1 Challenges involved with embedded HVDC link system	34
2.2 Project approaches	35
3 THEORETICAL ILLUSTRATION FOR POWER FLOW CONTROLS OF EMBEDDED HVDC	37
3.1 Formula derivation.....	39
3.2 VSC-HVDC model description.....	42
4 DESCRIPTION FOR THE EXAMINED BENCHMARK MODEL	45
5 INFLUENCE OF EMBEDDED HVDC ON SYSTEM PERFORMANCE	54
5.1 Critical mode test	54
5.2 Transient stability limit test	57
5.3 Dynamic performance analysis	60
6 CONCLUSIONS AND PROSPECTS	66
REFERENCES	68
APPENDIX	
A Dynamic Performance Diagrams	77

APPENDIX

B	Power Flow Data.....	92
C	Dynamic Data.....	95

CHAPTER 1

BACKGROUND INFORMATION AND LITERATURE REVIEW

With the constantly growing number of High Voltage Direct Current (HVDC) schemes worldwide, HVDC plays a more and more important role in Alternative Current (AC) system.

In spite of the recent improvements of power electronics, HVDC technologies continue to evolve from conventional thyristor-based system to voltage-source converter based HVDC (VSC-HVDC) system [1]. VSC-HVDC system represents the recent development of HVDC transmission technology [2]. In the recent decays, VSC-HVDC is able to resolve numerous issues which are difficult for AC system to analyze, including stabilizing the voltage in ac power network, reducing maximum fault currents level, and optimal management of electric power. Therefore the HVDC technology acts as an increasingly important role in the electric power industry [3].

The embedded HVDC system is an innovative concept which can be explained as an AC system consisting of HVDC links with at least two ends being physically connected within the synchronous ac network. With such a connection, it can perform not only the basic function of bulk power transmission, but also, more importantly, some additional control functions within the ac network such as power flow control, voltage control, system stability improvement and the mitigation of system cascading voltage [4].

The demand for more secure electric power grids and the increasing environmental concerns continue to drive researches in HVDC technology.

This thesis focuses on embedded HVDC systems; it analyzes the steady state stability issues and dynamic performance attached with such systems, therefore proposes

an optimal control scheme for embedded HVDC for the purposes of improving the performance and of enhancing both the stability and reliability of HVDC transmission.

1.1 State of the art

The first High Voltage Direct Current (HVDC) installations can date back to 1950s, when the 20MW, 100kV link between the Sweden mainland and the island of Gotland was commissioned [5]. The system took advantages over mercury arc valves, which required constant maintenance and rebuilding.

With the invention of high-voltage and large-power thyristor in the early 1970s, thyristor valves were gradually replacing the mercury arc valves. Thyristor valves have significantly increased system reliability with a reduced maintenance, which resulted in rapid developments of HVDC technology and the constructions of several HVDC systems in 1970s and 1980s [6]. After forty years developments, up to this decade, thyristor valve based HVDC is a mature, well-developed technology.

The recent breakthroughs in semiconductors are leading the revolutionary changes in HVDC technology, which bring the voltage source converter (VSC) based HVDC transmission system to reality. The world's first VSC-based HVDC system using pulse width modulation (PWM) IGBT converters was installed in March 1997 [11]. Since then, more VSC-HVDC systems have been installed worldwide [1].

1.1.1 Basic Configurations

There are several configurations to build a HVDC system. They are back-to-back configuration, monopolar configuration, bipolar configuration, and embedded HVDC configuration.

1.1.1.1 Back-to-back Interconnections

The back-to-back (B2B) link consists of two converters at the same site. And the converters are connected directly to each other without any transmission lines. This scheme is usually applied to asynchronous links where, two systems are in different frequencies or assorted control methods.

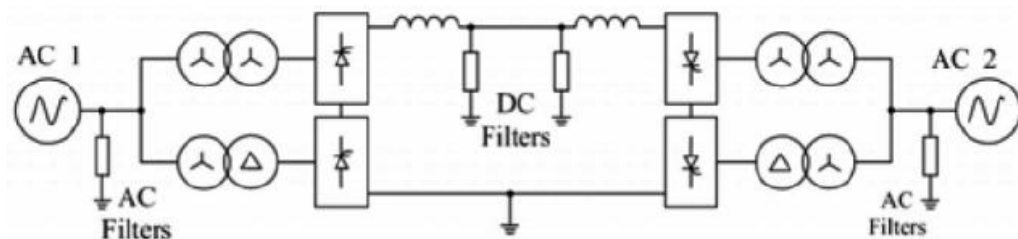


Figure 1 A Back-to-Back HVDC Configuration [6]

1.1.1.2 Monopolar Configuration

The monopolar link involves two converters connected with a single conductor. Earth or sea is normally used as the return conductor. When the system operates at the monopolar configuration, only a single conductor is performing at its operation voltage. When fault happens, high voltage transmission must stop working. Figure 2 shows a typical monopolar configuration.

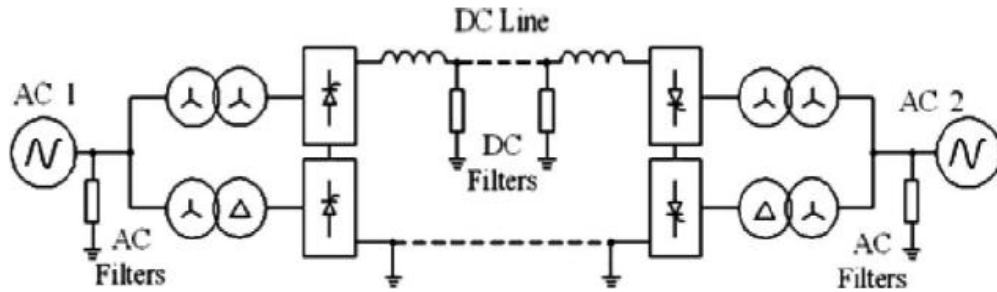


Figure 2 A Monopolar Configuration [6]

1.1.1.3 Bipolar Configuration

The bipolar configuration is the most widely used in HVDC system, because of the double insurance for the security of the system. During the failure operation of one DC line, the other DC line can still operate as a monopolar configuration for a certain time. In North America, monopolar configuration cannot be used for the stability restrictions, and all projects that can be applied in monopolar have been constructed in bipolar configurations.

In bipolar configuration, two monopolar systems are combined. One pole is positive and the other one is negative. One pole can continue to transmit power when the other one is out of service. Each pole can operate on its own as an independent system with the earth return. Figure 3 shows a typical bipolar configuration.

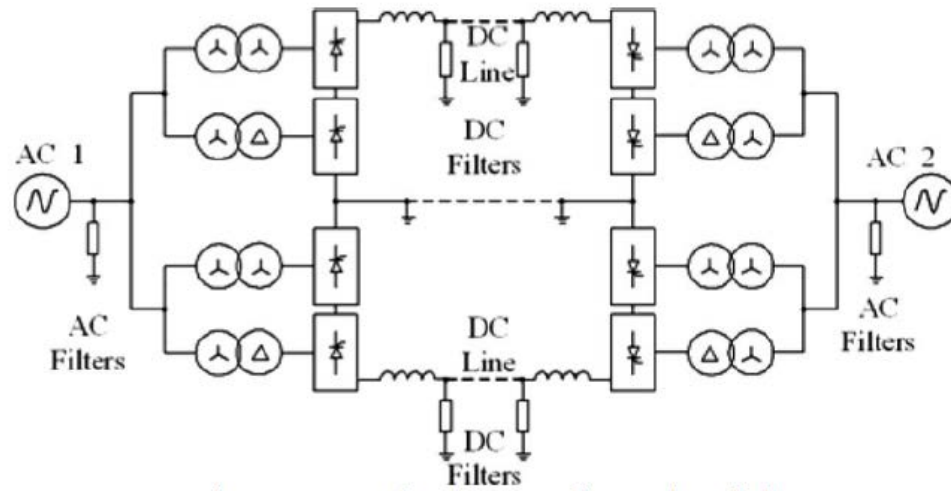


Figure 3 A Bipolar Configuration [6]

1.1.1.4 Embedded HVDC Configurations

The embedded HVDC system is a dc link with at least two terminals being physically connected within the synchronous ac network. From the figure below, the synchronous connected ac network could either be an AC transmission path or a meshed AC system (shown in figure 4). Meanwhile, the HVDC interconnections should be in a monopolar or a bipolar configuration, with a physically connected dc link.

With such a connection, it can perform not only the basic function of bulk power transmission, but also, more importantly, some additional control functions within the ac network such as power flow control, voltage control, system stability improvement and the mitigation of system voltage cascading failure.

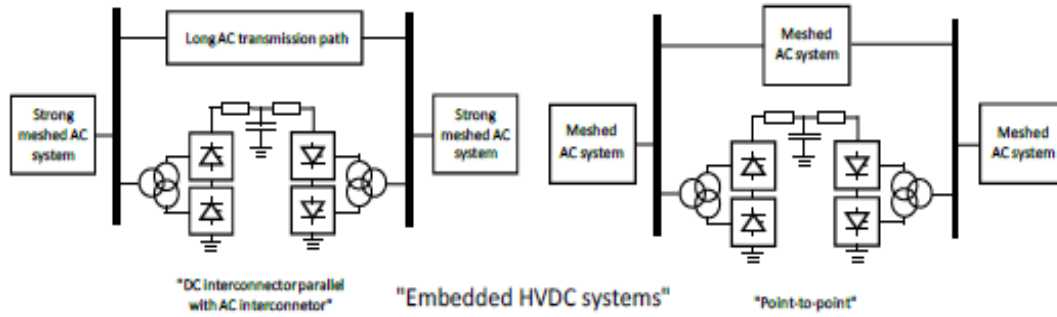


Figure 4 Embedded HVDC Configurations [4]

1.1.2 Descriptions of LCC-HVDC and VSC-HVDC, and feature comparisons

1.1.2.1 HVDC transmission using line-commutated current-source converters

The converter technology used for HVDC transmission in the early days was based on mercury valves. The major problem with mercury-arc technology was arc back failure which destroyed the rectifying property of the converter valve and consequently triggered other problems.

In the late 1960s, the thyristor valve technology was developed and overcame the problems of mercury-arc technology. Converters based on either mercury valves or thyristor valves are called line-commutated converters (LCC). The basic module of an LCC is the three-phase full-wave bridge circuit shown in Figure 5. This topology is known as the Graetz Bridge. Although there are several alternative configurations possible, the Graetz Bridge has been universally used as LCC-HVDC converters since it provides better utilization of the converter transformer and a lower voltage across the valve when not conducting [7].

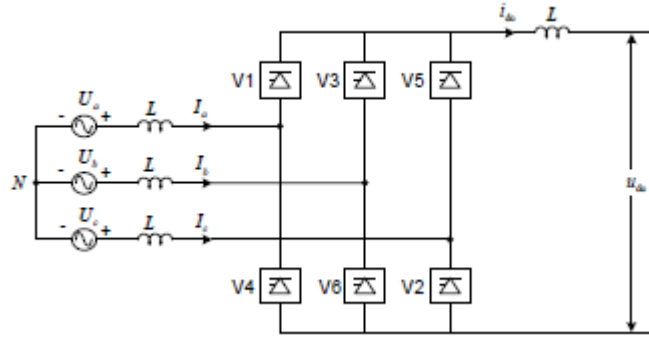


Figure 5 Graetz bridge for LCC-HVDC system

Graetz Bridge can be applied for transmitting power by two directions that the bridge is able to operate in the rectifier mode and the inverter mode. This can be achieved by setting up different firing angles on the thyristor valves. If the firing angle is lower than 90 degrees, the direct current will flow from the positive terminal of the dc circuit, thus the power will flow from the ac side to the dc side.

If the firing angle is higher than 90 degree, the direct voltage will change polarity, thus the direct current will flow from the negative terminal of the dc circuit. The power will then flow from the dc side to the ac side. An HVDC link is essentially constructed by two Graetz bridges, which are interconnected on the dc sides. The interconnection could be an overhead line, a cable, or a back-to-back connection.

LCC-HVDC links have been installed successfully and are expected to grow at least in the near future. However, the LCC technology suffers from several inherent weaknesses.

One problem is that the LCC always consumes reactive power, either in rectifier mode or in inverter mode. Depending on the firing angles, the reactive power consumption of an LCC-HVDC converter station is approximately 50-60% of the active

power. The reactive-power consumption requires compensation by connecting large ac capacitive filters at the converter stations. For a common LCC-HVDC link, the large filters not only increase the costs, but also occupy large amount of space of the converter stations. Additionally, they also contribute to the temporary overvoltage (TOV) and low-order harmonic resonance problems of the HVDC link when connected to a weak ac system [8].

Another well-known problem of the LCC-HVDC system is the occurrence of commutation failures (especially on the inverter side) caused by disturbances in the ac system. Either depressed voltage magnitude or phase-angle shift of the alternating voltage may reduce the extinction volt-time area of the inverter valve. If the extinction angle of the inverter valve is smaller than 5-6 degree, the previously conducted valve will regain current, which will end up with a commutation failure. Commutation failures are common phenomena of LCC-HVDC systems. A single commutation failure generally does no harm to either the converter valves or the ac system. However, a number of repeated commutation failures may force the HVDC link to trip [9].

While the above two problems can be mitigated by relatively easy measures, the third problem is more fundamental, which can become a limiting factor for LCC-HVDC applications. For LCCs, the successful commutation of the alternating current from one valve to the next relies on the stiffness of the alternating voltage, i.e., the network strength of the ac system. If the ac system has low short-circuit capacity relative to the power rating of the HVDC link, in other words, low short circuit ratio (SCR), more problematic interactions between the ac and the dc systems are expected. Besides, the

SCR of the ac system also imposes an upper limitation on the HVDC power transmission, which is often described by the well-known maximum power curve (MPC) [10].

As mentioned above, a LCC-HVDC link normally requires reactive-power compensation by connecting large ac filters at the converter stations. These filters will generate additional problems in weak ac systems, which will be described below. One such problem is the temporary overvoltage (TOV) issue. In case of a sudden change in the active power, or the blocking of converter, the large capacitors at the converter station together with the high inductance of the ac system cause a temporary overvoltage before the protection system disconnects the capacitors. TOVs can also lead to saturation of the converter transformer or transformers close to the dc station.

Another problem related to weak-ac-system connections is the low-order harmonic resonance. The high inductance of the ac system and the large filters of the HVDC link create a resonance of which the frequency tends to be lower for weak ac systems. Generally speaking, the lower the resonance frequency is, the greater the risk will be produced by harmful interaction with the converter control system.

An improved topology of the LCC-HVDC system to overcome part of the above mentioned problems is the capacitor-commutated converter (CCC)-HVDC technology, where ac capacitors are inserted in series between the valves and converter transformers. The series-connected capacitors not only supply the reactive power consumed by the valves, but also improve the dynamic performance of the HVDC system. However, the major drawback of the CCC concept is that the series capacitors increase the insulation costs of the valves. Thus, the CCC-HVDC technology has been so far only applied to back-to-back HVDC links, where the voltage level of the valves is much lower.

1.1.2.2 HVDC transmission using forced-commutated voltage-source converters

Voltage-source converters are a new converter technology for HVDC transmission [11]. The first commercial VSC-HVDC link with a rating of 50 MW was commissioned in 1997 in Gotland island of Sweden, close to the world's first LCC-HVDC link.

Voltage-source converters (VSCs) utilize self-commutating switches, such as, gate turn-off thyristors (GTOs) or insulated-gate bipolar transistors (IGBTs), which can be turned on or off freely, contrary to the LCC where the thyristor valve can only be turned off by being reversed line voltages. Therefore, a VSC can produce its own sinusoidal voltage waveform (using for instance pulse-width modulation (PWM) technology) independent of the ac system.

Many different topologies have been proposed for VSC. However, for HVDC applications, they have been so far limited to three major types: two-level converter, three-level converter, and modular multilevel converter (MMC) [1].

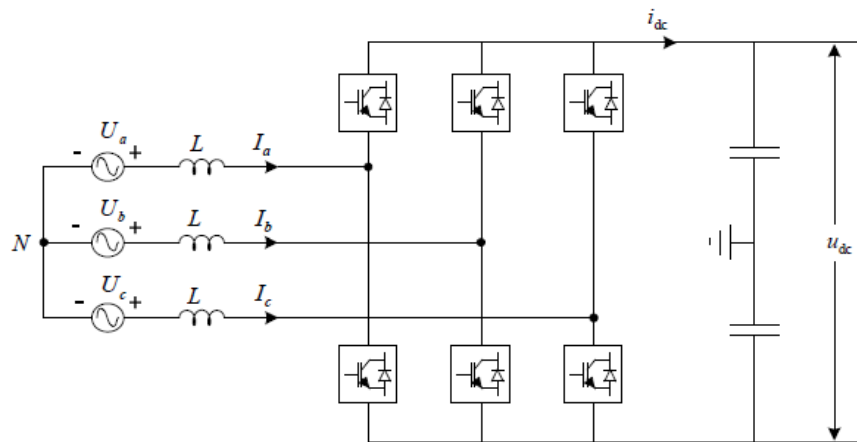


Figure 6 A two-level voltage-source converter

Figure 6 shows a two-level grid-connected VSC. The bridge consists of six self-commutating valves and each one consists of a switching device and an anti-parallel free-wheeling diode. For a typical HVDC link, two VSCs are interconnected on the dc side. In high voltage level applications, valves could be connected in series for a better operation. The control principle for the two-level bridge is fundamental, while each phase of the VSC can be connected either to the positive dc terminal, or the negative dc terminal. According to the reference voltage, the width of pulses could be modified to control the operation mode of VSC.

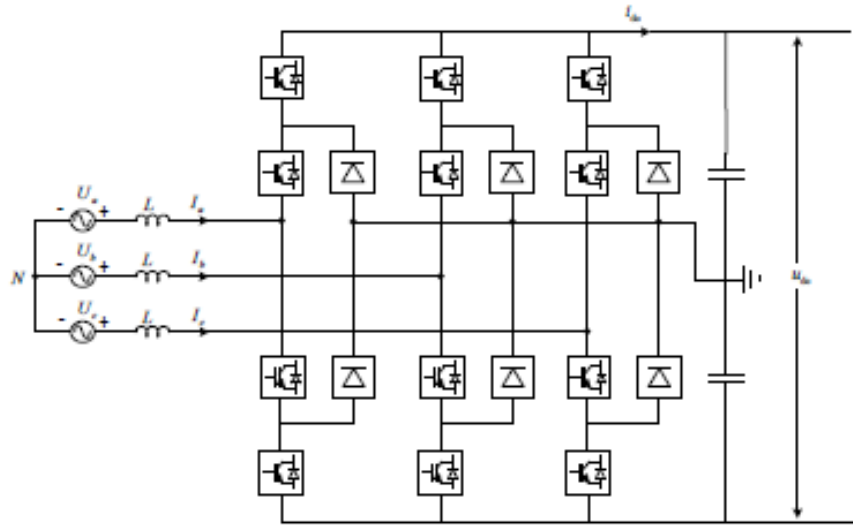


Figure 7 A three-level neutral-point-clamped (NPC) voltage-source converter

The three-level VSC shown above is also called neutral-point-clamped (NPC) converter. The key components that distinguish this topology from the two-level converter are the two clamping diodes in each phase. These two diodes clamp the switch voltage to half of the dc voltage. Thus, each phase of the VSC can switch to three different voltage levels, namely, the positive dc terminal, the negative dc terminal and the mid-point. Consequently, voltage pulses produced by a three-level VSC match closer to

the reference voltage. Additionally, the three-level NPC converter has lower switching losses. Compared with two-level VSCs, three-level NPC VSCs require more diodes for neutral-point clamping. However, the total number of switching components does not necessarily have to be higher. The reason for this is that, for HVDC applications, a valve consists of many series-connected switches. In the two-level case a valve has to withstand twice as high voltage than in the three-level case. Accordingly, the total number of switches is approximately equal. The NPC concept can be extended to a higher voltage level, which can result in further improved harmonic reduction and lower switching losses [12]. However, for high-voltage converter applications, the neutral-clamped diodes complicate the insulation and cooling design of the converter valve. Therefore, NPC concepts with a number of voltage levels higher than three have never been considered for HVDC applications [11]

The recently proposed modular multilevel converter (MMC) concept [12] attracts significant interests for high-voltage converter applications. Figure 8 shows the MMC topology for one phase. Compared with the above two topologies, one major feature of the MMC is that no common capacitor is connected at the dc side. Instead, the dc capacitors are distributed into each module, while the converter is built up by cascade-connected modules.

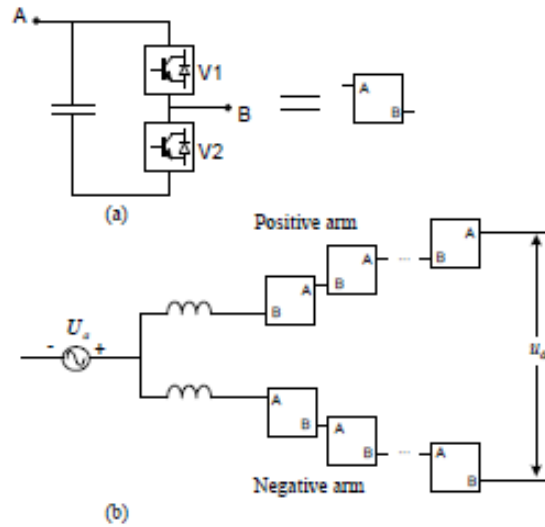


Figure 8 Modular Multilevel voltage-source converter. (a) One MMC module. (b) One phase topology.

The MMC concept is especially attractive for high-voltage applications, since the converter can be easily scaled up by inserting additional modules in each arm. If considerable amounts of modules are cascaded (approximately 100 modules would be common for HVDC applications), each module theoretically only needs to switch on and off once per period, which greatly reduces the switching losses of the valves. Nevertheless, in practical operation, a higher switching frequency is necessary. With MMC, the harmonic content of the voltage produced by the VSC is so low that additional filtering equipment is almost unnecessary.

An additional benefit of the MMC is that the control system has an extra freedom in dealing with faults at the dc side. The dc capacitors are not necessarily discharged during faults. Thus, the fault recovery can be faster.

Compared with the other two topologies, the major drawback of the MMC topology is that the required switching components are doubled since only one of the

valves of each module contributes to the phase voltage when the module is inserted in. Additional, the design for a MMC topology will involve more complex controls than the two-level converter. However, since the switching frequency of the MMC can be kept very low, switches with higher blocking voltages may be used, which in turn limits the increase in a number of switches. On the other hand, the reduction of switching losses and savings on filtering equipment of the MMC can justify its application for HVDC transmission.

VSC-HVDC technology overcomes most of the weaknesses of the LCC-HVDC technology. In addition, it supports the ac system with reactive-power supply/consumption independently from the active power order (except for highest values). The figures below represent typical P/Q capabilities for VSC converters, for 2-level and MMC topologies.

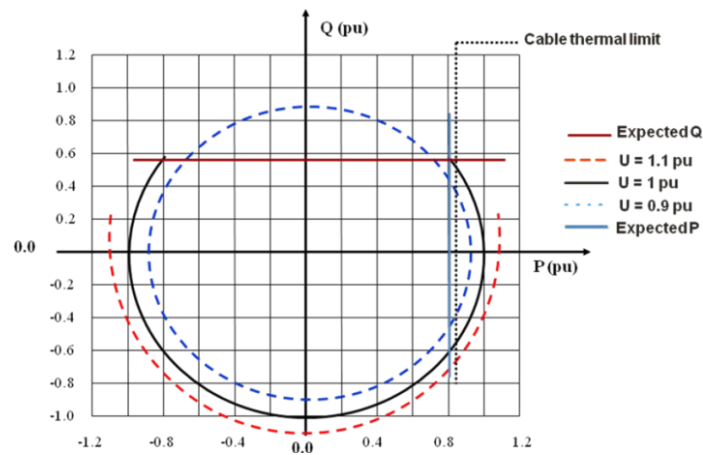


Figure 9 Typical P/Q capability for 2-level VSC converters.

Similar to a LCC-HVDC system, the VSC-HVDC system can quickly run up or run back the active power for ac system emergency-power support, but it can also instantly reverse the active power by adjusting the voltage level at each terminal [13].

Since the direct voltages of a VSC-HVDC system are comparatively much smaller than those in LCC-HVDC system, the extruded cable is able to be applied in VSC-HVDCs. The extruded cable reduces both the cable cost and the construction investment. And this cable has made the long-distance land-cable transmission possible [14].

1.1.2.3 Feature comparisons between LCC-HVDC and VSC-HVDC systems.

Compared with classical HVDC, the VSC-HVDC has following advantages:

- 1) An advanced power flow control capability, which allows rapid reversals of power flow direction by current polarity changes;
- 2) A capability of multi-terminal interconnection;
- 3) The avoidance of commutation failures due to disturbances in AC network.
- 4) A capability to independently control active and reactive flows at each terminal by the converters;
- 5) A possibility of connecting the VSC-HVDC system to a “weak” ac network or even to one where no generation source is available, and naturally, the short-circuit level is very low.
- 6) No need of transformers to assist the commutation process of the converter’s fully controlled semiconductors.
- 7) A faster dynamic response due to higher PWM frequency than the fundamental switching frequency (phase-controlled) operation, which further results in reduced need for filtering, and hence smaller filter size.
- 8) A capability of paralleled operation of DC network on regional AC grid.

- 9) A reduced construction and commissioning time for a HVDC system.

Table 1 summarizes the main features between classical HVDC and VSC-HVDC technology.

Table 1 Comparison of Classical HVDC and VSC-HVDC [15]

Attributes	Classical HVDC	VSC-HVDC
Converter technology	Thyristor valve, grid commutation	IGBT valve, self-commutation
Max converter rating at present	6400 MW, ± 800 kV (overhead line)	1200 MW, ± 320 kV (cable)
Relative size	4	1
Typical delivery time	36 months	24 months
Active power flow control	Continuous ± 0.1 Rated Power to \pm Rated Power (Due to the change of polarity, normally changing the power direction takes some time, which is not the case for VSC-HVDC)	Continuous 0 to $\pm P_r$
Reactive power demand	Reactive power demand = 50% power transfer	No reactive power demand
Reactive power compensation & control	Discontinuous control (Switched shunt banks)	Continuous control (PWM built-in in converter control)
Independent control of active & reactive power	No	Yes
Scheduled maintenance	Typically < 1%	Typically < 0,5%
Typical system losses	2.5 - 4.5 %	4 - 6 %
Multi-terminal configuration	Complex, limited to 3 terminals	Simple, no limitations

1.1.3 Control methods of VSC-HVDC system

A VSC-HVDC system usually consists of three parts: a rectifier station, an inverter station and HVDC transmission lines or cables. Figure 9 shows a simplified

HVDC light configuration with two terminals. Each terminal connects to an AC system by equivalent impedance representing the converter transformer and reactor between the VSC and the ac system.

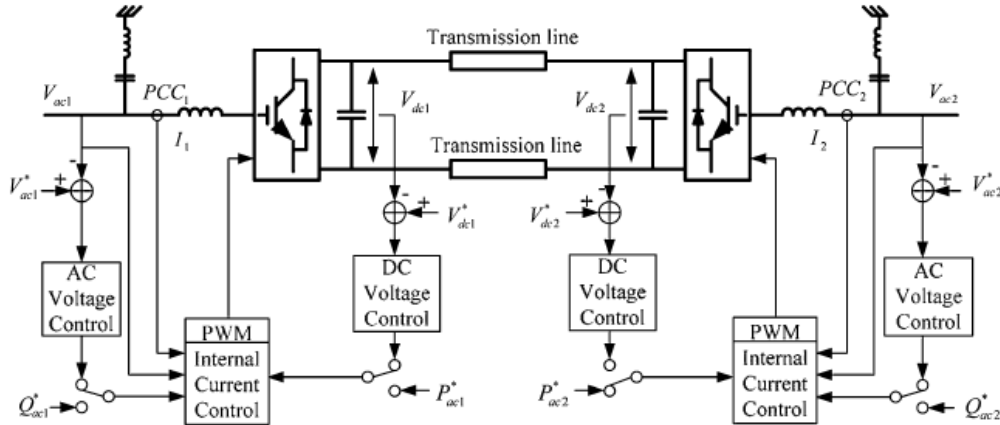


Figure 9 Configuration of a HVDC light transmission system [16]

Normally, each VSC is able to control its reactive power independently. However, the active power flow must be balanced, which means that the active power entering the HVDC system must be equal to the power leaving it plus the power losses in the DC transmission system. In order to achieve this balance, one of the VSC stations have to control the DC voltage and the other VSC station is designed for active power control.

Figure 11 shows the equivalent system model of a VSC station.

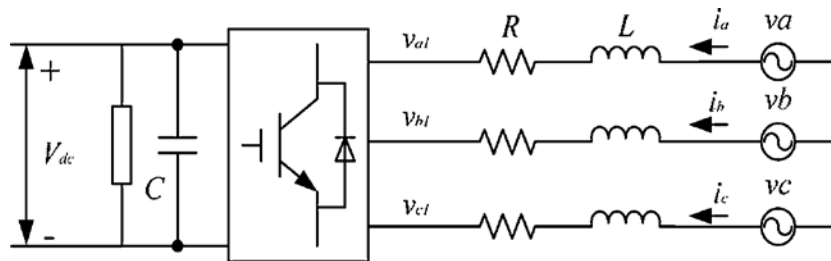


Figure 10 Equivalent system model of a VSC station [16]

According to Figure 10,

$$\begin{bmatrix} v_d \\ v_q \end{bmatrix} = R \begin{bmatrix} i_d \\ i_q \end{bmatrix} + L \frac{d}{dt} \begin{bmatrix} i_d \\ i_q \end{bmatrix} + \omega_s L \begin{bmatrix} -i_q \\ i_d \end{bmatrix} + \begin{bmatrix} v_{d1} \\ v_{q1} \end{bmatrix}, \quad (1)$$

Where

ω_s is the angular frequency of the AC system. v_d , v_q , v_{d1} , and v_{q1} represent the d and q components of the PCC voltages and the VSC output voltages, respectively. The currents i_d and i_q represent the d and q components of the current flowing between the ac system and the VSC.

Equation (1) could be expressed by a complex equation (2) using space vector.

Under steady-state, (2) becomes (3)

$$V_{dq} = R * i_{dq} + L \frac{d}{dt} i_{dq} + j\omega_s L * i_{dq} + v_{dq1}, \quad (2)$$

$$V_{dq} = R * I_{dq} + j\omega_s L * I_{dq} + V_{dq1}, \quad (3)$$

The instantaneous active and reactive powers transferred from the ac system to the VSC are proportional to the d-axis and q-axis currents, respectively, as shown by (4) and (5).

$$p_{ac}(t) = v_d i_d + v_q i_q = v_d i_d, \quad (4)$$

$$q_{ac}(t) = v_q i_d - v_d i_q = -v_d i_q, \quad (5)$$

The current flow from the ac system to VSC is:

$$I_{dq} = \frac{V_{dq1} - V_{dq}}{jX_L} = \frac{V_{d1} - V_d}{jX_L} + \frac{V_{q1}}{X_L}, \quad (6)$$

in which, $X_L = j\omega_s L$ is the reactance of the converter transformer and reactor between the VSC and the PCC.

And the power transfer from ac system to VSC could be

$$P_{ac} + jQ_{ac} = V_{dq} I_{dq}^* = V_d I_{dq}^*, \quad (7)$$

By solving (6) and (7), (8) (9) are obtained.

$$P_{ac} = -\frac{V_d V_{q1}}{X_L}, \quad (8)$$

$$Q_{ac} = \frac{V_d}{X_L} (V_d - V_{d1}), \quad (9)$$

The conventional VSC control of an HVDC light system has a nested-loop structure consisting of a faster inner current loop and a slower outer control loop that generates d-axis and q-axis current references i_d^* and i_q^* to the current loop controller [17].

Now, the VSC is used for active-power control, the d-axis current reference, according to (4), is:

$$i_d^* = \frac{P_{ac}^*}{V_d}, \quad (10)$$

where, P_{ac}^* is the desired active power transferred from the ac to the dc system, and if the VSC is used for dc voltage control, the d-axis current reference is generated by a dc voltage loop controller [18][19].

For reactive-power control, the q-axis current reference, according to (5), is

$$i_q^* = \frac{-Q_{ac}^*}{V_d}, \quad (11)$$

where, Q_{ac}^* is a desired reactive power of the ac system.

Figure 10 shows the overall conventional d - q vector control structure, in which the VSC is used for dc voltage control. The d and q reference voltage, v_{d1}' and v_{q1}' , include the d and q voltage, v_d' and v_q' , from the current-loop controllers plus the compensation terms shown in (12) and (13). The two reference voltages, v_{d1}^* and v_{d1}^* , are

used to generate a set of three-phase sinusoidal reference voltage, v'_{a1} , v'_{b1} , and v'_{c1} to control the PWM converter.

$$v_{d1}^* = -v'_d + \omega_s L_{i_q} + v_d, \quad (12)$$

$$v_{q1}^* = -v'_q - \omega_s L_{i_d}, \quad (13)$$

It is possible that d- and q-axis current and voltage reference generated by the nested-loop controller may exceed the physical constraints of the VSC. Although rate limiters could be applied to the reference inputs to limit the changing rates of the controller output signals, those rate limiters cannot prevent the current and/or voltage signals generated by the nested-loop controller from exceeding the physical constraints of the VSC.

As a result, the following strategies are used in the design of the nested-loop control system [16]:

- 1) In order to prevent the converter from entering the nonlinear modulation mode, a saturation mechanism is applied to the output voltage of the controller if the amplitude of the reference voltage generated by the controller exceeds the PWM saturation limit. The general strategy is to set limitations for $|v_{d1}^*|$ and $|v_{q1}^*|$, but keeping $\angle v_{d1}^*$ and $\angle v_{q1}^*$ unchanged, as shown by (14),(15) [20][21].

$$\angle v_{d1_new}^* = V_{\max} * \cos(\angle v_{dq1}^*), \quad (14)$$

$$\angle v_{q1_new}^* = V_{\max} * \sin(\angle v_{dq1}^*), \quad (15)$$

- 2) To prevent the converter from exceeding the rated current, the q-axis current is adjusted if the amplitude of the reference current generated by the dc

voltage and reactive-power control loops exceeds the rated current limits. The general strategy is keeping the d-axis current reference unchanged to maintain dc voltage control effectiveness while modifying the q-axis current reference to satisfy the reactive-power control demand as much as possible, as shown by (16)(17)[20][21]

$$i_{d_new}^* = i_d^*, \quad (16)$$

$$i_{q_new}^* = \text{sign}(i_q^*) * \sqrt{(i_{dp_max}^*)^2 - (i_d^*)^2}, \quad (17)$$

1.2 Existing embedded HVDC descriptions

1.2.1 Caprivi link (Namibia)

The SAPP (Southern African Power Pool) represents an ac interconnected Power System with three HVDC systems. Major generation situated in South Africa consists mainly of thermal Power Stations, while the Eastern Corridor (Zimbabwe and Zambia) contains mainly Hydro Power Stations. The Western Corridor (Namibia) has only very small Hydro and thermal generation. As the main scope of this document is of embedded HVDC systems in AC networks, more focus will be given to Caprivi Link that is situated in Namibia and was completed in June 2010. This Link forms a very important regional interconnection in the South African Power Pool. It should be noted that the Cahora Bassa HVDC scheme also has a parallel ac network path between the converter stations. A Grid Master Power Controller has been implemented to control power flows between

the parallel dc and ac paths. This controller is especially important during contingency situations.

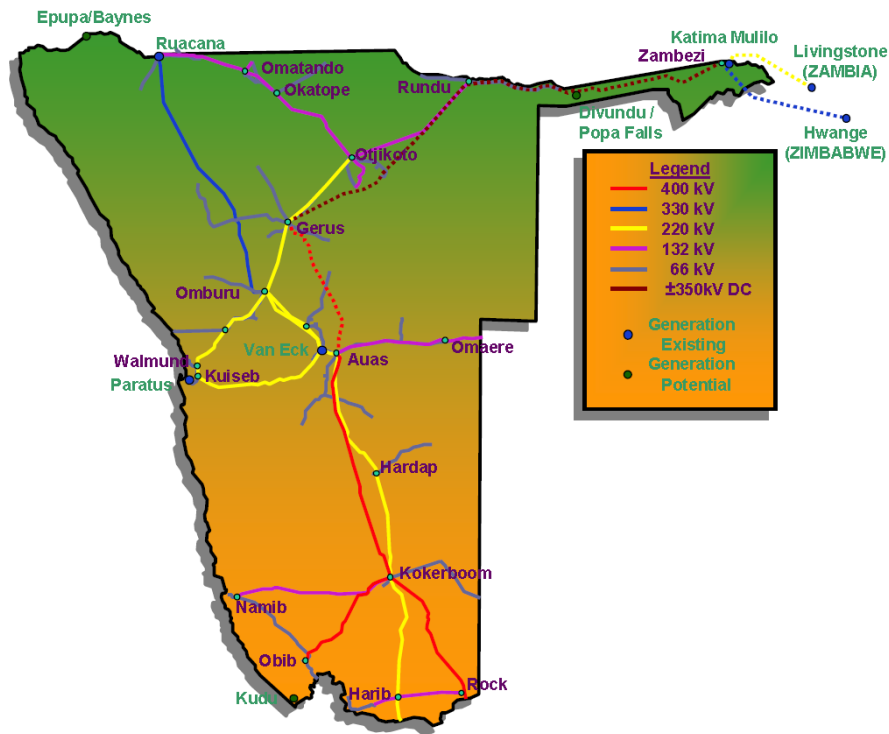


Figure 11 Geographic Location of Terminal Points for the Caprivi Link Interconnector (The figure is directly taken from [22])

The Caprivi monopole scheme (rated at 300 MW) connects the electricity networks of Namibia and Zambia. The Zambezi 330 kV substation near Katima Mulilo in the Caprivi Strip is connected to Gerus 400 kV substation near Otjiwarongo in the centre of Namibia with 950 km of overhead line operating at 350 kV dc. The scheme utilizes Voltage Sourced Converters (VSC) and is the first scheme to use VSC technology with overhead lines. The Link has been designed to allow for a future bipole extension (300 MW) in conjunction with ac network strengthening which is planned to connect Zambezi 330 kV substation to Botswana and Zimbabwe and a 400 kV line from Gerus to Auas substation in the central part of Namibia.

The scheme connects two presently very weak ac networks where the fault levels can be as low as 0.8 of the rated power of the converters. The presently weak networks have a high possibility of transferring to islanded/passive ac networks such as when the Kafue Town – Victoria Falls transmission line in Zambia trips and about 100MW generation at Victoria Falls islands together with the Zambezi Converter. A similar condition can occur on the Gerus (Namibian) side when the ac link to South Africa is lost and the converter islands together with Ruacana Hydro Station. Similarly both sides can experience passive conditions where no generation is present in the island. Without the HVDC link being installed, the outage of critical lines can easily lead to an eventual blackout of the area due to the extremely weak ac network conditions.

The Voltage Source Converter HVDC has proven to enhance stability and assist with the prevention of blackouts when two extremely weak ac networks are interconnected and run in parallel with an ac network such as the South African Power Pool. It provides very robust voltage support when inherent voltage collapse situations arise while giving stable frequency support to island or passive network conditions, thereby preventing eventual blackout. It also caters for the diverse network conditions that are planned for the future eventual providing n-1 network security when the bi-pole is implemented.

1.2.2 Kii Channel HVDC Project (Japan)

Electricity transmission system in Japan is a special system because the country is divided into two regions each operating at a different main frequency. Eastern Japan (including Tokyo, Kawasaki, Sapporo, Yokohama, and Sendai) runs at 50 Hz; Western

Japan (including Okinawa, Osaka, Kyoto, Kobe, Nagoya, Hiroshima) runs at 60 Hz. The frequency difference partitions Japan's national grid. As a result, the power can only be transmitted between the two parts of the grids using frequency converters, or HVDC transmission lines [23].

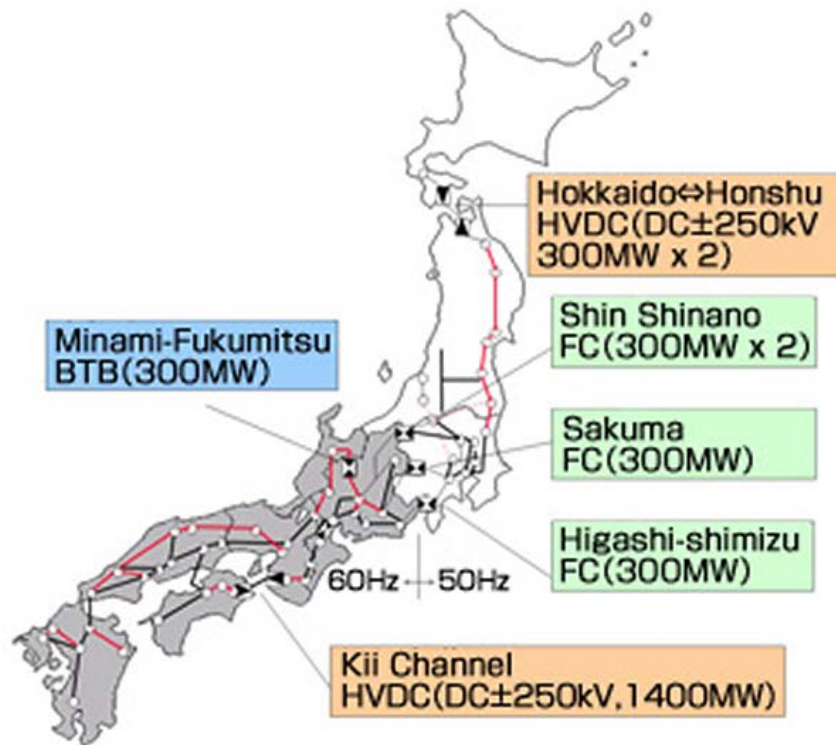


Figure 12 HVDC transmission system in Japan [24]

The first entire HVDC project having DC transmission line was Hokkaido – Honshu HVDC Link connecting between Hokkaido Island and Honshu Island. As the second entire HVDC project, Kii Channel HVDC Project interconnecting between Honshu Island and Shikoku Island was commissioned in 2000 for transmitting power generated at coal fired thermal power plants which consisted of two units of 1050MW and one unit of 700MW located in Shikoku Island. Kii Channel HVDC Project was

planned, constructed and co-owned by Kansai Electric Power Company (KANSAI), Shikoku Electric Power Company (SHIKOKU) and Electric Power Company [25].

The configuration of Kii Channel HVDC project shown in below figure is one bi-pole having rates of 1400MW, 250kV and 2800A at the first stage, and 2800MW, 500kV and 2800A at the final stage but not implemented yet.

1.2.2.1 Configuration of Kii Channel HVDC Link

The configuration of Kii Channel is one bi return circuit is metallic return system to avoid and to mitigate environmental impact as far as possible. Pole circuit component such as DC bus, overhead transmission, submarine cable and smoothing reactors were designed and constructed for DC 500kV use. Fig. 11 which covers mainly largest load center, Osaka city. Contractors/manufactures for converter systems are Toshiba for Pole#1 and Hitachi for Pole#2 of Anan End, and Mitsubishi for Pole#1 and Hitachi for Pole#2 of Kihoku End respectively.

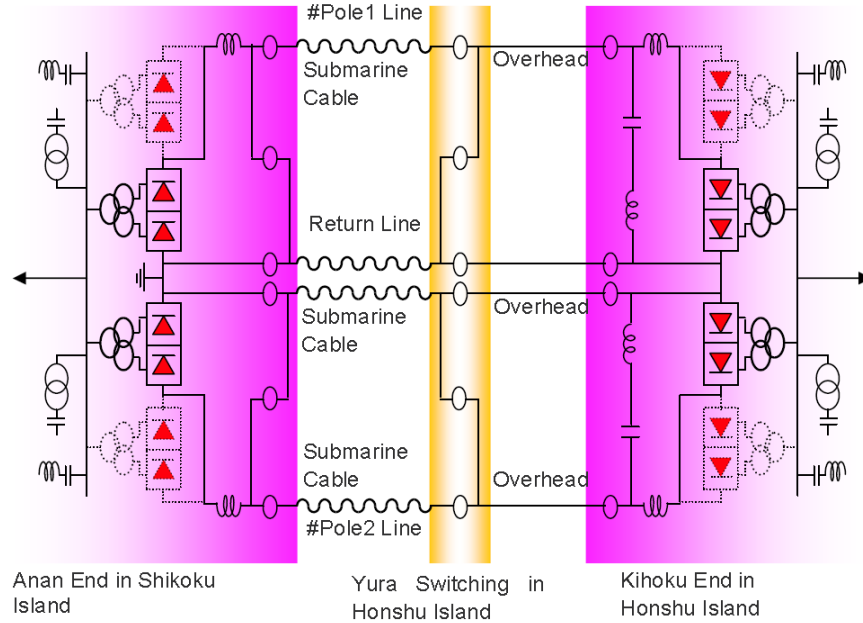


Figure 13 Kii Channel HVDC configuration [25].

1.2.2.2 Operation Principles

This HVDC project uses Line Commutated Converter technology which is the preferable to effectively transport reliable large power with combining overhead transmission line and submarine cable. Because of requirements of huge power and reliable transportation, various new technologies not only for main circuit equipment but also for control system were applied to this HVDC project.

1.2.3 Kingsnorth HVDC Link (England)

The Kingsnorth HVDC transmission project at one time was the only application of HVDC scheme to be "embedded" in an existing AC network [26].

The National Grid in the UK first originated in the 1930s with a transmission voltage of 132 kV used to interconnect the hitherto independent regional electricity generating and supply companies. At first, the 132 kV lines were lightly loaded, since most electricity continued to be generated close to where it was being used, but gradually a shift towards larger, centralized power generating stations located close to the source of fuel (mostly coal) took place. In the 1950s a higher transmission voltage of 275 kV was introduced to re-inforce the grid and in the early 1960s the first parts of the 400 kV transmission network had been built.

Each of the three largest cities (London, Birmingham and Manchester) was served by a 400kV outer ring, with radial connections inwards to an inner ring at lower voltage. In London, a new coal-fired power station (Kingsnorth) was being built during the 1960s on the Thames estuary to the East of the city, feeding into the outer ring. Nonetheless, significant planning problems were being encountered in injecting the power generated by this station into the centre of the city.

Accordingly the Central Electricity Generating Board (CEGB), the then-nationalized electricity utility for England and Wales, placed an order in 1966 for a 640 MW underground cable HVDC link from the Kingsnorth power station to two sites in South and West London. The objective was to feed the receiving stations and support the adjacent AC system without increasing the short-circuit level.

The Kingsnorth station consisted of two poles, each with a power transmission rating of 320 MW at 266 kVdc and consisting of two series connected 6-pulse groups of mercury-arc valves. Both the Beddington and Willesden stations were single poles rated at 320 MW and consisting of two 6-pulse groups. A neutral DC cable linked the

Willesden and Beddington stations and, together with changeover switchgear, permitted power to be transmitted between these two stations in the event of the cable from Beddington to Kingsnorth being out of service. The Kingsnorth link had a total length of 82 km (underground cable).

The Kingsnorth scheme was commissioned in 1972 and contained many “firsts” for HVDC. It was the first HVDC scheme to be “embedded” in an existing AC system, as opposed to interconnecting two separate AC systems. It was also the first HVDC scheme to use entirely land cables for power transmission. Mercury arc valves were ARBJ/6 type and were the largest mercury arc valves (in both voltage and current ratings) ever built by any manufacturer. Replacement of mercury arc valve with air cooled thyristor valve occurred in 1981. The Kingsnorth scheme was decommissioned in 1987.

1.2.4 Fenno-Skan (Finland-Sweden)

In addition to synchronous AC tie-lines to Sweden and Norway, Finland is connected with neighboring transmission networks using five HVDC systems. Four of those given in Table 2 can be considered to be a part of the Finnish transmission networks whereas Vyborg b2b LCC-HVDC, which connects the asynchronous Nordic and Russian transmission networks, is located in Russia nearby city of Vyborg.

Table 2 The HVDC systems in Finland.

<i>Name</i>	<i>Embedded HVDC</i>	<i>In operation since or Planed start of operation</i>	<i>Length (km)</i>
Fenno-Skan	Yes	1989	200(Submarine)
EstLink	No	2003	130(Submarine)
Fenno-Skan2	Yes	Q4/2011	200(submarine)+70(OHL)
EstLink2	No	Q1/2014	130(Submarine)+30(OHL)+10(Land Cable)

In order to explain the role of the two Fenno-Skan HVDC systems considering the dynamics of the Nordic AC transmission network, the structure and certain dynamic characteristics of the Nordic transmission system must be described in short. As illustrated in figure 15, the Fenno-Skan HVDC connections are in parallel with AC transmission path with length of order 2000 km and they basically connect the South Finland and South Scandinavia. Due to length of the transmission path between the South Finland, that is both the main area of generation and consumption, and South Scandinavia, AC power transfer from and to South Finland is actually limited by stability phenomena; under South to North power flow conditions by damping of 0.3 Hz inter-area oscillations and under North to South conditions voltage stability [29].

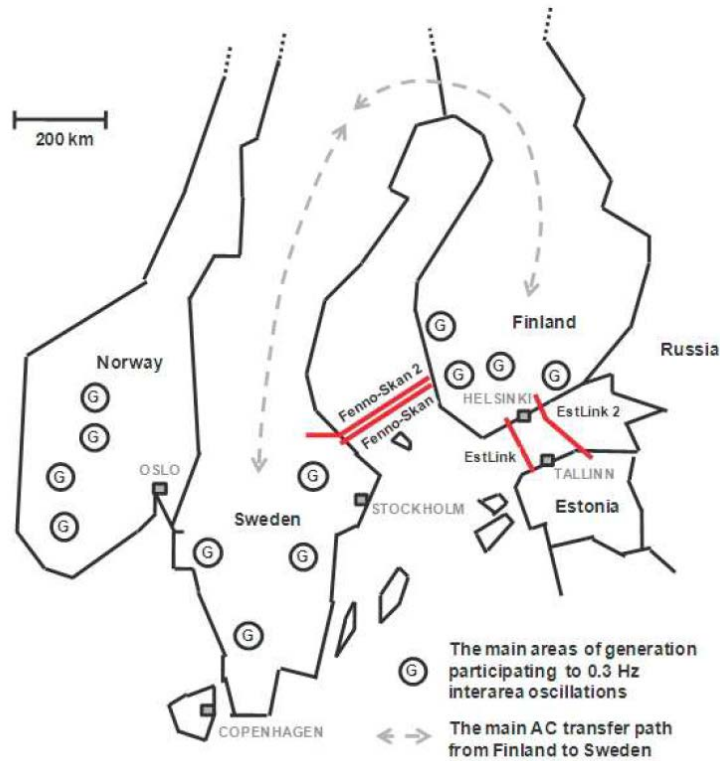


Figure 14 HVDC connections in Finland and their contribution on AC system.

With respect to both stability phenomena the location of Fenno-Skan HVDC is nearly ideal considering the contribution of HVDC controls on dynamic performance of the AC network. As Fenno-Skan HVDC systems basically connect two areas, where two main groups of generators oscillating against each other in 0.3 Hz inter-area mode are located, the controllability of the Fenno-Skan POD controls over this 0.3 Hz mode can be considered very good. The main contribution of Fenno-Skan HVDC to voltage stability phenomena is based on the fact that under certain power flow conditions it offers a possibility to relieve the level of AC transmission towards South Finland. Some of such conditions related to weakened voltage stability initiate the emergency power control sequences that are designed automatically to decrease the AC power flows.

With respect to interactions between the AC system and HVDC system, two additional concepts have been applied in operation of Fenno-Skan and will be applied in operation of Fenno-Skan 2; the optimization of North to South power transfers and the subsynchronous damping controls.

1.2.5 Directlink (Australia)

Directlink is an embedded VSC link that connects Mullumbimby (New South Wales) and Bungalora (Queensland) in Australia. It is part of the Terranora interconnector between the two areas, which features AC and DC components [30].



Figure 15 Geographic Location of Directlink

Picture is directly taken from [31].

Directlink was commissioned in 2000 and formed the first intertie between New South Wales and Queensland. It was initially established as a merchant link to take advantage of the energy price differentials in the market between Queensland and New South Wales. At the time the load growth in the south east of Queensland was outpacing

the development of energy sources and energy prices were escalating. Since then the much larger capacity AC link (Queensland to New South Wales Interconnector – QNI) has been commissioned and Directlink has been converted to a regulated asset. Both Directlink and QNI now operate in parallel and are dispatched by the Australian Energy Market Operator (AEMO).

Directlink is constructed of 3 parallel VSC links each rated at 60MW providing a total capacity of 180MW. The links operate at +/-80kV rated DC and are 59km long. The 3 links are identical in nature and operate independently from one another.

HVDC technology was selected for this project given the need for power flow control, especially as this was the only intertie between the two large AC systems at the time. Furthermore the AC networks where the link would be connected were relatively weak, with approximately 120-180MW of capability and quite low fault levels. VSC technology was selected primarily given the low fault levels at either end of the link, as well as the need for a compact solution offering minimal environmental impact. It was realized at the time that the lost opportunity resulting from extended delays due to overhead environmental approval processes would not be economically attractive for the developer.

1.2.6 Guizhou–Guangdong I & II (China)

The HVDC long-distance transmission system of Gui-Guang transmits 3,000 MW of power from the Anshun substation in Guizhou Province in southwest China to the Zhaoqing converter station in Guang-dong Province near the load center of Guangzhou.

It is a bipolar system, each pole comprising a 12-pulse converter bridge suspended from the ceiling. The thyristors are water-cooled and direct-light-triggered. The converter transformers are of the single-phase two-winding type. Triple-tuned filters are used for filtering harmonics on the DC- and AC-side of the converters. The smoothing reactors are of the oil-immersed type. Commercial operation of this HVDC link started in October 2004.

The DC Transmission Project (the long-distance transmission system of the Guizhou-Guangdong II line ± 500 kV) transmits 3,000 MW power from the Xingren substation in the Guizhou Province of South-west China to the load center of Shenzhen in the Guangdong Province (under exploitation in 2007). The system has a long-term overload capability of up to 115%. Power transmission in the reverse direction is also possible.

The bipolar system is designed for a ceiling suspended 12-pulse converter bridge arrangement with single-phase two-winding converter transformers and oil-insulated smoothing reactors. The 500 kV DC converter groups of modular design are equipped with direct light-triggered thyristors with water cooling. Most of the DC equipment is provided with composite housings improving the performance of operation under severe environmental conditions.

For harmonic filtering triple tuned AC and DC filters are used. The design considers the installation at 1450 m above sea level (Xingren converter station). The inter connection of the neutrals of both stations is implemented by means of ground electrodes.

CHAPTER 2

SYSTEM TECHNICAL PERFORMANCE ISSUES WITH EMBEDDED HVDC LINKS

As a novel technology with traditional features, there are numerous challenges associated with this technology. In this chapter, several challenges involved with the embedded HVDC will be proposed.

2.1 Challenges involved with embedded HVDC link system

The first challenges involved with embedded HVDC link is the reliable robust models and control theory for the system. Numerous models for traditional HVDCs have been developed; nevertheless, extensive system studies require the incorporation of the embedded HVDC models in different system planning programs, power flows, dynamic performances, small signal stability and other programs so that appropriate controls and advanced VSC station topologies may be developed. The above requirements necessitate the modification and upgrade of the available HVDC models, so that they can be seamlessly integrated across time-scale applications. Each model must capture the pertinent dynamic behaviors of the time-scale in which it is deployed.

The second challenge is the capability of embedded HVDC and current AC networks. As embedded HVDC links cannot work stand alone from AC networks. The studies for static stability, power flows, and transient stability of embedded HVDC link cooperation with existing facilities in AC system, such as FACTS devices, circuit breakers, and renewable energy resources become important. Also, the capability of

HVDC power transmission and the influence of HVDC on HADC power transfer capability need to be studied.

2.2 *Project Approaches*

1) Task 1: Derivation of Embedded HVDC Models

The literature on embedded HVDC system is still fairly sparse since this technology is relatively new. Most reports are on specific applications and do not develop VSC station topologies or controls in a systematic manner. Accurate dynamic models are an essential component of developing system level controls such as oscillation damping and transient stability improvement, nevertheless up till now, few in terms of modeling embedded HVDC system have been reported. The thesis develops a detailed model of embedded HVDC system in terms of conventional d-, q- vector control. The model is a detailed model and capable of analyzing power flow, static stability and system dynamic performance.

2) Task 2: Improvement of embedded HVDC control topologies and models improvement

System topologies and control methods of embedded HVDC system need to improve to further increase system stability and obtain maximum power transmission. New technology in power electronics and power flow control methods can be applied to embedded HVDC system. The thesis determines a new control method of power oscillation control. The proposed control mechanism employs the angular frequency at two VSC station terminals as reference input, with PI controls.

3) Task 3: System performance evaluation

The thesis evaluated the dynamic performance of embedded HVDC system by conventional d-, q- vector controls and the system with new control topologies. A six-bus four machine system is depicted as a sample, the comparison among the system transmission with HAVC, embedded HVDC with conventional d-, q- vector control, and embedded HVDC with derived control topology.

CHAPTER 3

THEORETICAL ILLUSTRATION FOR POWER FLOW CONTROLS OF EMBEDDED HVDC

Compared to AC infrastructures, HVDC lines offer the possibility to set and control active power flows going through them. Figure 16 describes an equivalent model of a VSC-HVDC system, which consists of two VSC stations. One station works as a rectifier while the other operates as an inverter. Each VSC station has two degrees of control freedom. One degree is used for reactive-power control, while the other degree is used for active power or dc voltage control.

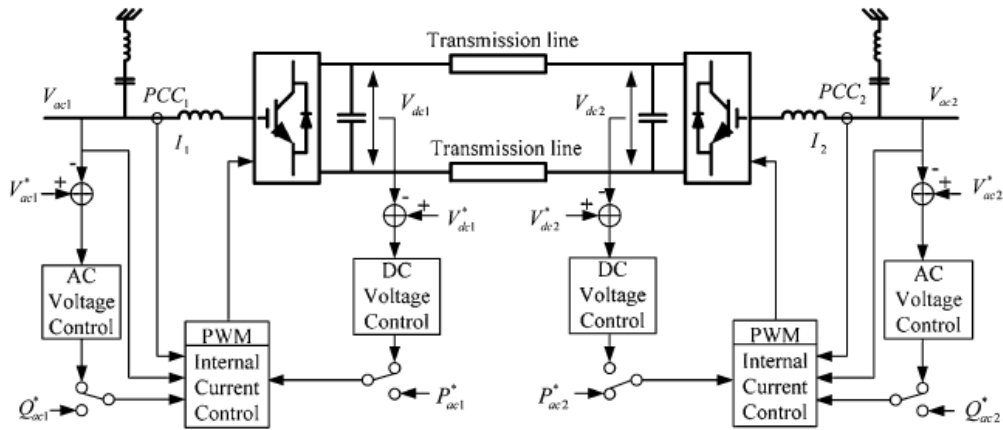


Figure16 Configuration of a HVDC light transmission system [15]

(Duplicated copy of Figure 9)

As shown in Figure 16, the VSC-HVDC system allows fully independent control of active and reactive powers within the operating range of the design. Technically, each VSC station is able to control its reactive power, and voltage level independent of the other station. However, the active power flow in dc transmission must be balanced, that the active power entering the HVDC system must be equal to the power leaving it plus

the losses in the system. In order to summit the balance, one of the VSC stations is designed to control the DC voltage, and the other one is for active power control.

Under the VSC-HVDC transmission system d-q reference frame depicts in chapter 1, the ac system active and reactive powers P_{ac} and Q_{ac} are controlled through q and d components V_{q1} and V_{d1} of the VSC voltage onto the ac system. The P_{ac} and Q_{ac} and be represented as:

$$P_{ac} = -\frac{V_d V_q}{X_L}, \quad Q_{ac} = \frac{V_d}{X_L} (V_d - V_{d1}).$$

If the VSC is used for active power control , the basic principle is that under the VSC rated power and PWM saturation constraints, the system should be operated to achieve the active power control goal while minimizing the difference between the reference and actual reactive powers.

In embedded HVDC systems, the interconnections between the ac system are not only DC transmissions but also ACs, therefore, the frequencies at two VSC-station AC ends should be exactly the same. The frequency difference will results in instability of the transmission system. In order to minimize the active power oscillation $P_{osc} = |P_{ac} - P_{ac}^*|$ in the DC transmission system, the frequency difference between the two VSC station AC ends can be set an reference input to minimize the active power oscillation P_{osc} .

The following parts of this chapter depicts formula derivation of this control principle, also a six-bus four-machine system equipped with embedded HVDC system by the specific control method is described.

3.1 Formula derivation

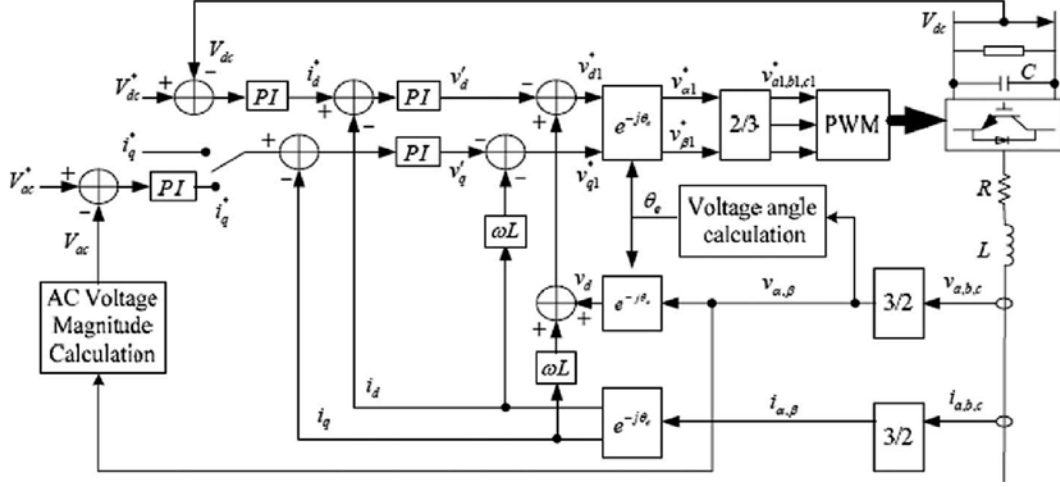


Figure 17 Conventional d-, q- vector control structure [16]

A typical configuration of VSC HVDC transmission control structure is shown in Figure 17. The figure shows an overall traditional d-q vector control structure [18], where the VSC is used for DC voltage control.

Rewrite the equation (12) and (13),

$$v_{d1}^* = -v_d' + \omega_s L i_q + v_d, \quad (18)$$

$$v_{q1}^* = -v_q' - \omega_s L i_d, \quad (19)$$

The d and q reference voltage, v_{d1}^* and v_{q1}^* , include the d and q voltage, v_d' and v_q' , from the current-loop controllers plus the compensation terms shown in (12) and (13). The two reference voltages, v_{d1}^* and v_{q1}^* , are used to generate a set of three-phase sinusoidal reference voltage, v_{a1}^* , v_{b1}^* , and v_{c1}^* to control the PWM converter.

In order to further improve the dynamic performance of the embedded HVDC to the system, a power control loop can be introduced to the system.

According to equation (10), $i_d^* = \frac{P_{ac}^*}{V_d}$, the reference P_{ac}^* can be substitute in to

$$P_{ac}'' = P_{ac}^* + P_{comp}, \quad (20)$$

where,

P_{ac}^* is a fixed value, according to the power system demand;

P_{comp} is an extra power reference, which is designed to compensate power oscillations in the system.

The power transfer between two ac system network is :

$$P = \frac{E_1 E_2}{X_{12}} \sin(\delta_1 - \delta_2), \quad (21)$$

where,

E_1 and E_2 is the AC voltage magnitude at each VSC terminal,

δ_1 and δ_2 is the phase angle at each VSC terminal.

$$P_{osc} = P - P_0 = \frac{E_1 E_2}{X_{12}} [\sin(\delta_1 - \delta_2) - \sin(\delta_{10} - \delta_{20})], \quad (22)$$

because, $(\delta_1 - \delta_2) = (\omega_1 - \omega_2) * t + (\delta_{10} - \delta_{20})$

$\sin(\delta_1 - \delta_2) - \sin(\delta_{10} - \delta_{20})$ can be represented as,

$\sin[(\omega_1 - \omega_2) * t + (\delta_{10} - \delta_{20})] - \sin(\delta_{10} - \delta_{20})$.

As a result,

$$\begin{aligned} P_{osc} &= \frac{E_1 E_2}{X_{12}} \sin(\delta_1 - \delta_2) \\ &= \frac{E_1 E_2}{X_{12}} \{ \sin[(\omega_1 - \omega_2) * t + (\delta_{10} - \delta_{20})] - \sin(\delta_{10} - \delta_{20}) \}. \end{aligned}$$

$(\delta_{10} - \delta_{20})$ is a constant depending on the initial condition of the phase angles difference between the terminals of the two VSC terminals, hence $\sin(\delta_{10} - \delta_{20})$ is also a constant.

$(\omega_1 - \omega_2)$ is the frequency difference of the two system. The frequencies are time dependent variables; therefore the frequency difference between the two systems is a time dependent variable.

$$\text{Assume } \omega_{\Delta} = \omega_1 - \omega_2 ; k_1 = \frac{E_1 E_2}{X_{12}} ; k_2 = \delta_{10} - \delta_{20} ; k_3 = k_1 * k_2$$

$$\begin{aligned} P_{osc} &= k_1 * [\sin(\omega_{\Delta} * t + k_2) - k_2] = k_1 * \sin(\omega_{\Delta} * t + k_2) - k_3 \\ &= k_1 * [\sin(\omega_{\Delta} * t) * \cos k_2 + \sin k_2 * \cos(\omega_{\Delta} * t)] - k_3 \end{aligned}$$

in S domain

$$\mathcal{L}(P_{osc}) = P_{osc} = k_1 * \cos k_2 * \frac{\omega_{\Delta}}{s^2 + \omega_{\Delta}^2} + k_1 * \sin k_2 * \frac{s}{s^2 + \omega_{\Delta}^2} - \frac{k_3}{s}, \quad (23)$$

From (23) the oscillation power flow in S-domain between the two system can be represented as a function of s and ω_{Δ} , where, ω_{Δ} is an independent input derived from the system.

In order to eliminate the power flow oscillation, installing a real-time controlled power reference P_{cmp} subtracted from active power reference can compensate the P_{osc} dynamically. According to equation (23), the P_{cmp} can be set up as a function of ω_{Δ} , the frequency difference between the two HVdc terminals.

In S-domain, the compensation power, P_{cmp} can be represented as:

$$P_{cmp} = \text{controller} * (\Omega_1 - \Omega_2),$$

in which, Ω_1 and Ω_2 is the AC system angular frequency at each HVDC terminals.

As a result, the expected new power oscillation between the two area with an installed compensatory real power reference can be represented as:

$$P_{osc} - P_{cmp}.$$

Assume the overall active power through the HVDC transmission is the summation of a constant active power and active power oscillation. Therefore with the compensation power, the real power flow will be $P_{overall} = P_{const} + P_{osc} - P_{cmp}$. One of the targets in this project is to reduce the value of $P_{osc} + P_{comp}$ and make it as small as possible. And with a input reference of frequency difference, the depicted embedded HVDC dynamic performance is largely improved. A detailed simulation model is to be described in the following part of this chapter and in the next chapter.

3.2 VSC-HVDC model description

As described in previous chapters, VSC-HVDC system mainly consists of three parts: rectifier station, inverter station and transmission lines. Figure 18 shows a typical VSC-HVDC topology, including rectifier and inverter. The power transfer direction is from rectifier to inverter. Figure 19 shows the topology of VSC-HVDC in rectifier, and Figure 20 shows the topology of VSC-HVDC in inverter. Therefore, an inverter station topology is the same as a rectifier topology, but the power transfer direction is opposite.

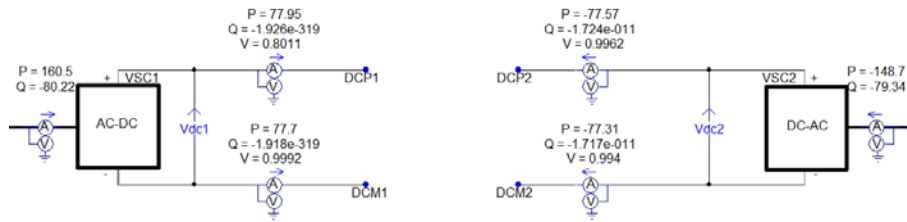


Figure 18 VSC-HVDC topology

In order to balance the active power, the real power entering the rectifier equals to the power leaving the inverter plus the power losses on the DC cables and VSC stations.

For the controls for the rectifier and the inverter, voltage reference will be set to a fixed value at rectifier side and the voltage at inverter side will be automatic adjusted to meet the power flow demand.

For the conventional d-, q- vector controls of VSC-HVDC, the power reference is a fix value at inverter end. Therefore the power reference at rectifier end will automatic be fixed to be the value equals to the overall power through inverter end plus the power losses on DC cables.

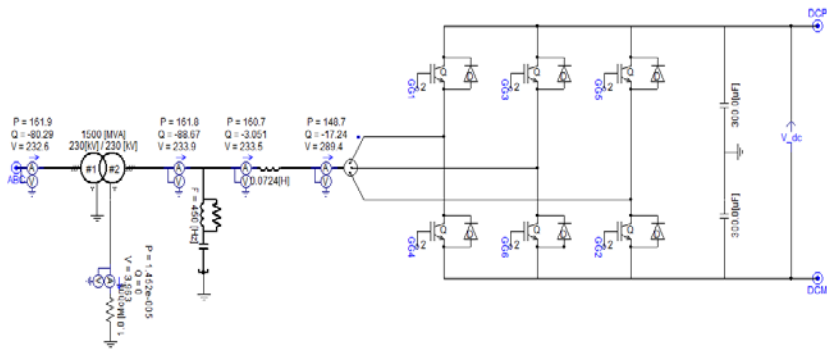


Figure 19 Rectifier topology of VSC-HVDC

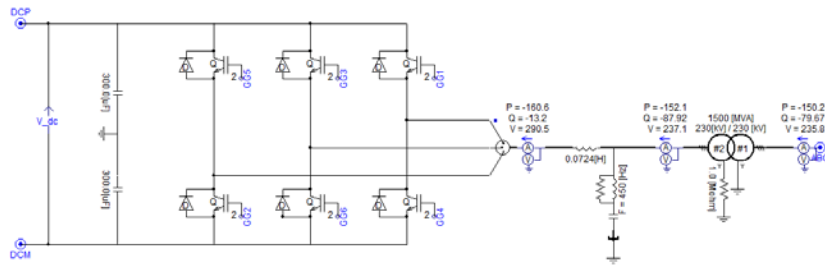


Figure 20 Inverter topology of VSC-HVDC

In order to further improve the system dynamic performance, a power oscillation controllers applied in spite of the inverter power input reference. As shown in Figure 21, the input to the controller is the frequency difference between the two VSC station terminals, and the output is the power reference to the inverter station. A PI controller is

utilized, and a limiter is also applied to constrain the compensation power, so that the extra investment regarding this control method is able to be estimated.

According to the equation,

$$P_{comp} = (\omega - \omega_2) * (K_p + \frac{K_i}{s}) \quad (24),$$

the frequency difference between rectifier station and inverter station could be the reference for the compensation power control.

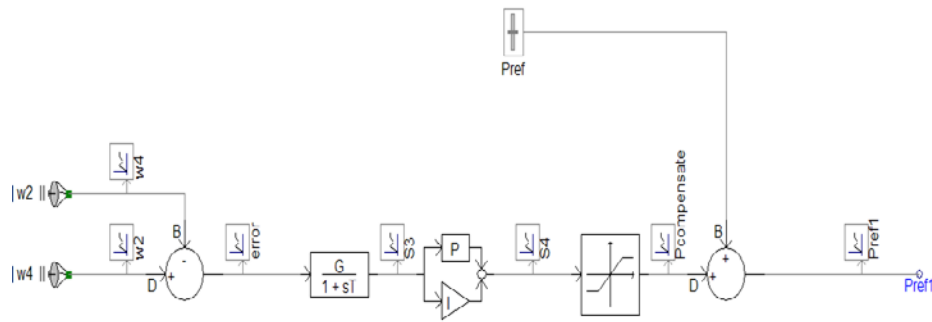


Figure 21 Block diagram of compensate power control

The diagram above briefly describes a compensate power control system in S domain. The input is the frequency difference which is followed by a low pass filter, an PI controller, and a limiter. P_{ref} is the same as P_{ac}^* in (16), Pref1 is the power reference to the inverter.

The limiter has comparatively small values for both lower and upper limits, therefore, the compensation power would varied in a small scale, $\pm 5\%$ in this project. Compared to the power transmission between two areas, the compensation power is small. And the cost for the build of the power controller would be tiny, while compared with the total investment on VSC station.

CHAPTER 4

DESCRIPTION FOR THE EXAMINED BENCHMARK MODEL

In order to examine the system steady state and dynamic performance, the IEEE 6-bus 4-machine system, rated at 230kV, is performed as a test system. The system has four synchronous machines and two dynamic loads. A schematic diagram for the system is shown in Figure 22.

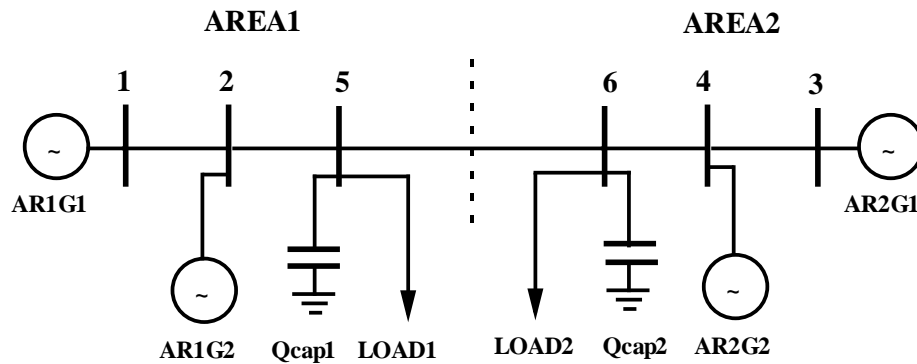


Figure 22 A schematic diagram of 6-bus 4-machine system

The following parts depict each device applied in the system.

4.1 Generator

The generator model in use is IEEE standard fossil steam unit, F20, rated at 896MVA and 26kV. The generator simulations are described by two-axis models.

Therefore all values for sub-transient variables are approximated to zero.

The generator variables are listed below:

$$R_a=0.0025 \quad X_d=1.8 \quad X_q=1.7 \quad X_l=0.20 \quad X'd=0.3$$

$$X'q=0.55 \quad X''d=0.25 \quad X''q=0.25 \quad T'd0=8.0 \quad T'q0=0.4$$

$$T''d0=0.03 \quad T''q0=0.05$$

H1=6.5 H2=6.5 H3=6.175 H1=6.175

Figure 23 illustrates the detailed parameters for generator settings in PSCAD

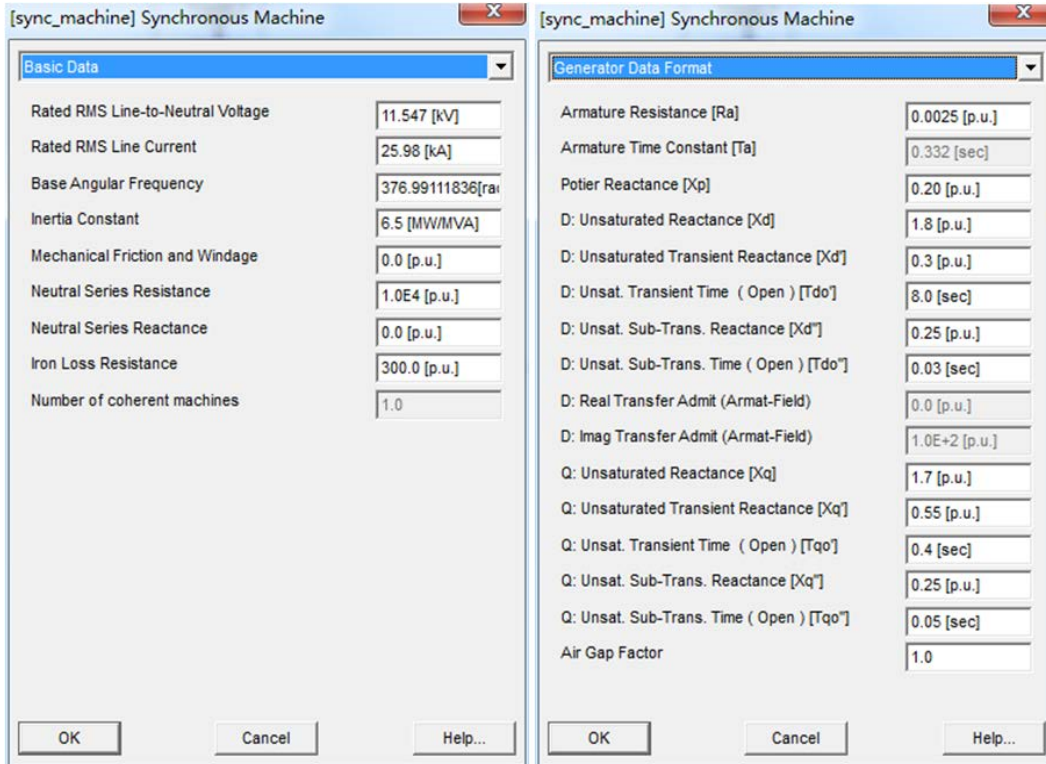


Figure 23 Detail parameters for generator setting in PSCAD

4.2 Exciter

Exciter model in use is IEEE(1992/2005) AC4A exciter. The exciter variables in use are the default values. Figure 24 shows the block diagram of AC4A excitation system, and Figure 25 show the detailed parameter setting in the model.

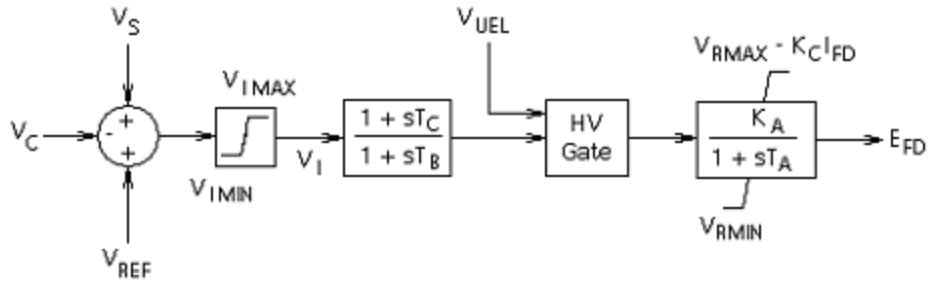


Figure 24 AC4A excitation system block diagram

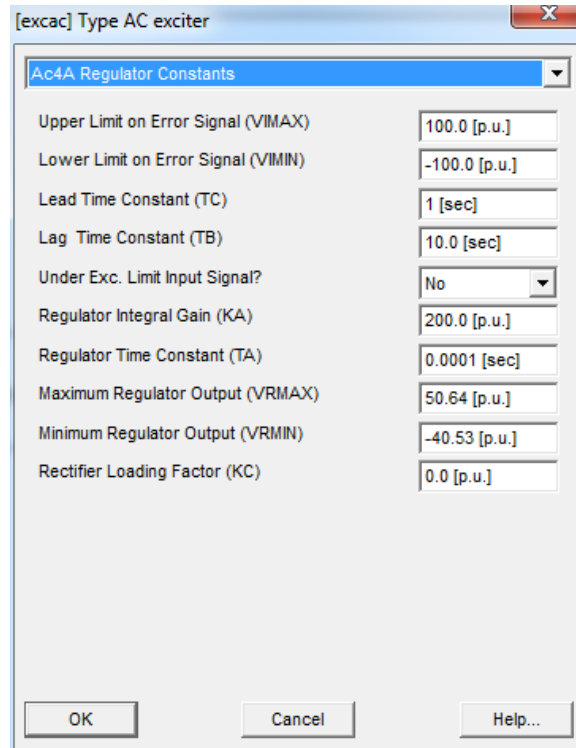


Figure 25 Detail parameters for exciter setting in PSCAD

4.3 Power System Stabilizer(PSS)

The generator model also employs a PSS to stabilize the frequency. The block diagram of PSS is shown in Figure 26, and Figure 27 shows the detail parameters, in which $K_{s1}=4.5$ and $T_{s1}=15$.

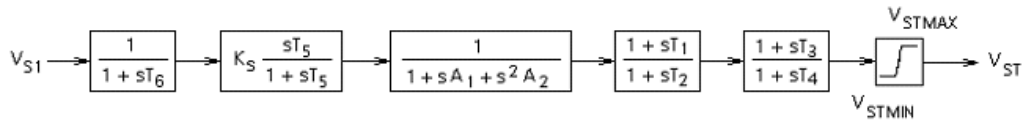


Figure 26 Power System Stabilizer (PSS) block diagram

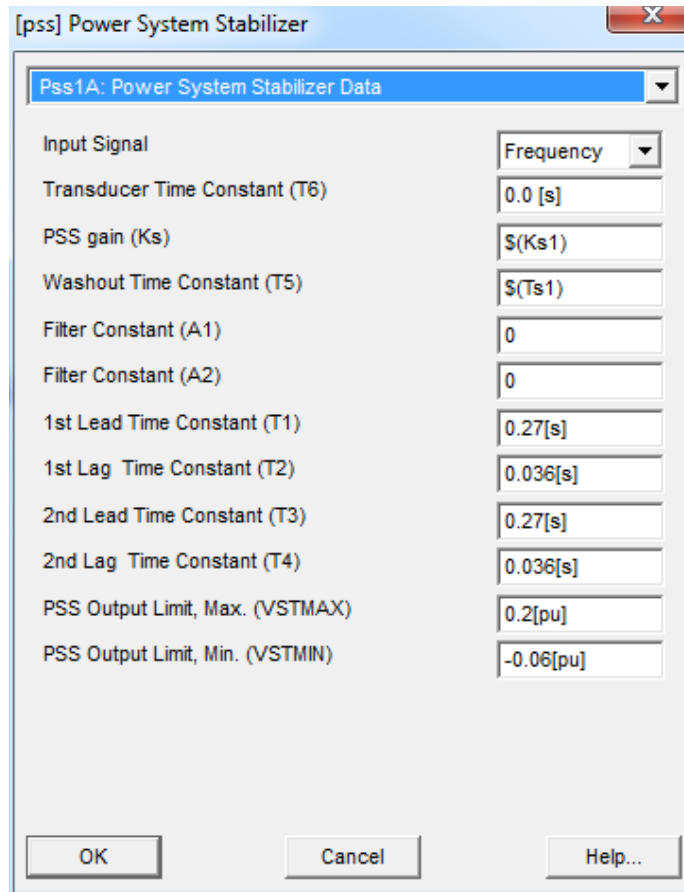


Figure 27 Detail settings for PSS model

4.4 Generator, Exciter, PSS, Transformer Connections

Figure 28 shows the connection of generator, exciter and transformer used in the testing system. Therefore generators will finish the initialization in 0.7 second and will

connect to the grid at 1.0 second. Meanwhile, transformer models, with taps, are added into the system, which defaults at 1.0.

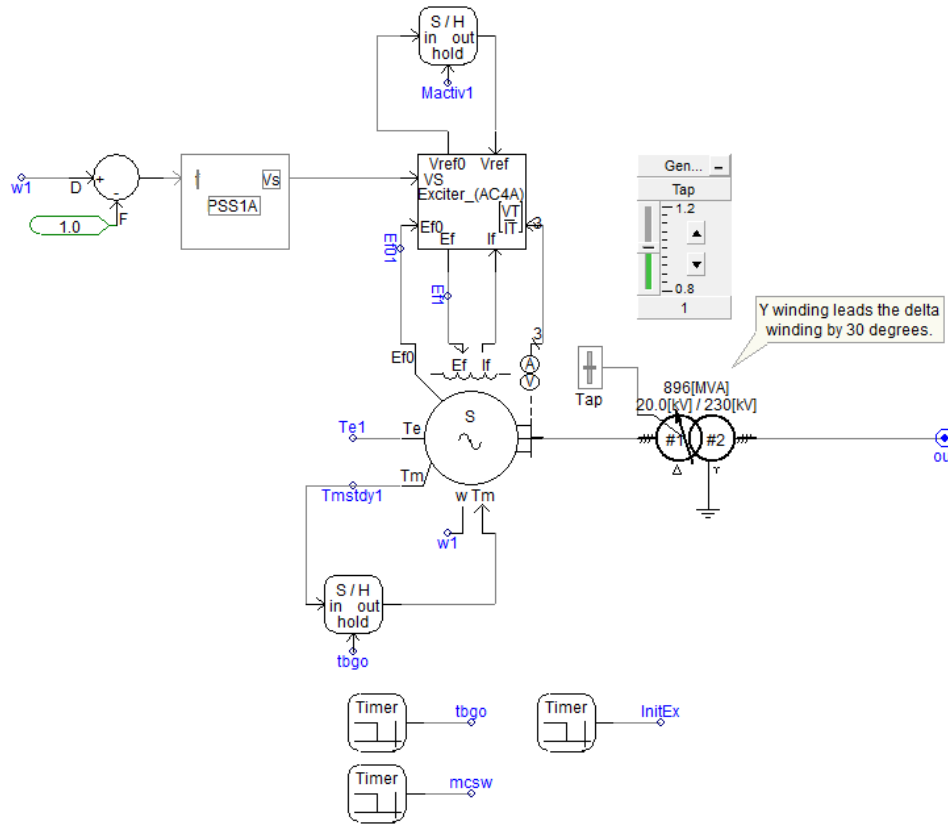


Figure 28 Diagram of connection among generator, exciter, PSS and transformer

4.5 AC transmission Line

The transmission line is modeled as coupled PI section with resistance, inductive reactance and capacitive susceptance. And the line is rated at 60 Hz, under the 100 MVA based system. The transmission line parameters are listed in Table 3.

Table 3 Transmission line parameters

<i>Rated Voltage L-L</i>	<i>230 [kV]</i>
+ve Seq. Resistance	0.1E-6 [p.u./m]
+ve Seq. Inductive Reactance	1.0E-6 [p.u./m]
+ve Seq. Capacitive Susceptance	1.7E-6 [p.u./m]
0 Seq. Resistance	0.1-6 [p.u./m]
0 Seq. Inductive Reactance	1.0-6 [p.u./m]
0 Seq. Capacitive Susceptance	1.7E-6 [p.u./m]

The distance between each bus is based on power flow data for 6-bus 4-machine system in appendix. A brief description is given in Table 4.

Table 4 Length of transmission lines

<i>From Bus</i>	<i>To Bus</i>	<i>Distance</i>
1	2	25.0E3 [m]
2	5	10.0E3 [m]
5	6	220.0E3 [m]
6	4	10.0E3 [m]
4	3	25.0E3 [m]

4.6 Load

The load is modeled by a three phase fixed load in connection with a three phase capacitive load. The fixed loads are in delta connection and rated at 60 Hz.

The fixed load models the load characteristics as a function of voltage magnitude and frequency, where the load real and reactive power considered separately by using the expressions:

$$P = P_0 * \left(\frac{V}{V_0}\right)^{NP} * (1 + K_{PF} * dF),$$

and,

$$Q = Q_0 * \left(\frac{V}{V_0}\right)^{NQ} * (1 + K_{QF} * dF).$$

Where,

P is the equivalent load real power,

P_0 is the rated real power per phase,

V is the load voltage

V_0 is the rated load voltage (RMS, L-G value)

$NP = \frac{dP}{dV}$ is the index for real power

$K_{PF} = \frac{dP}{dF}$ is the frequency index for real power

Q is the equivalent load for reactive power

Q_0 is the rated reactive power (plus inductive) per phase

$NQ = \frac{dQ}{dV}$ is the voltage index for reactive power

$K_{QF} = \frac{dQ}{dF}$ is the frequency index for reactive power

The voltage index for real power ($\frac{dP}{dV}$) is set to 1, voltage index for reactive power ($\frac{dQ}{dV}$) is set to 2, frequency indexes for both real and reactive power are set to 0.

Figure 29 shows a typical load model schematic.

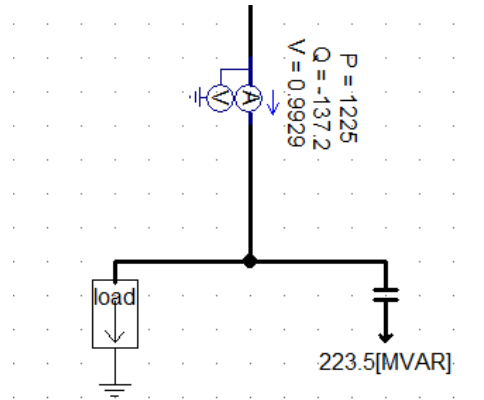


Figure 29 Load model schematic

4.7 HVDC Cable

The HVDC cable transmission is an alternative solution for long distance power transmission. The cable may transmit power instead of AC transmission line respectively, or transmit power paralleled with AC line. The HVDC cable is the 300kV dc cable, and the HVDC cable in use is a Bi-polar topology, so conductors are taken into applications in the study.

The cable model is shown in Figure 30. An equivalent circuit of cable model is revealed in Figure 31 [33]. The length of the DC cable is determined the same as AC transmission line.

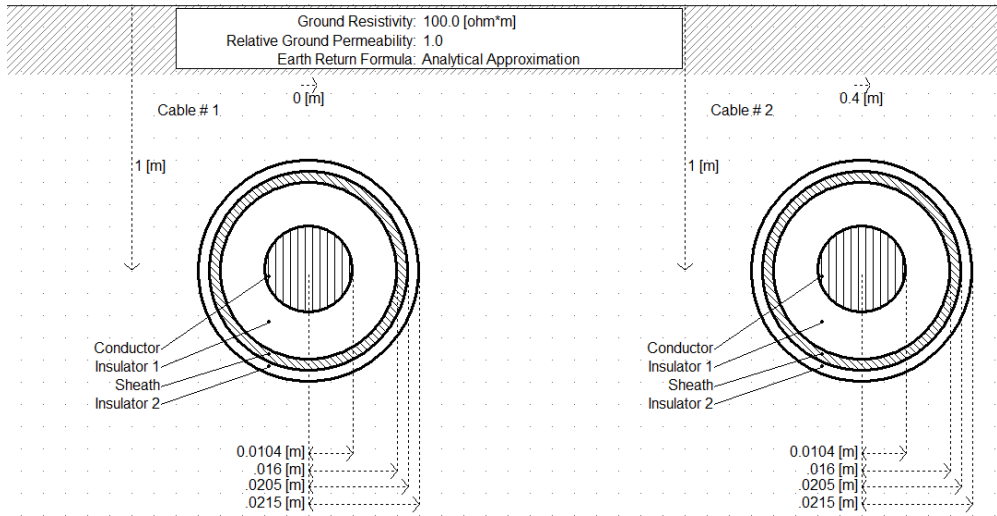


Figure 30 An example of HVDC cable model used in simulation study

[Screen shot from PSCAD program]

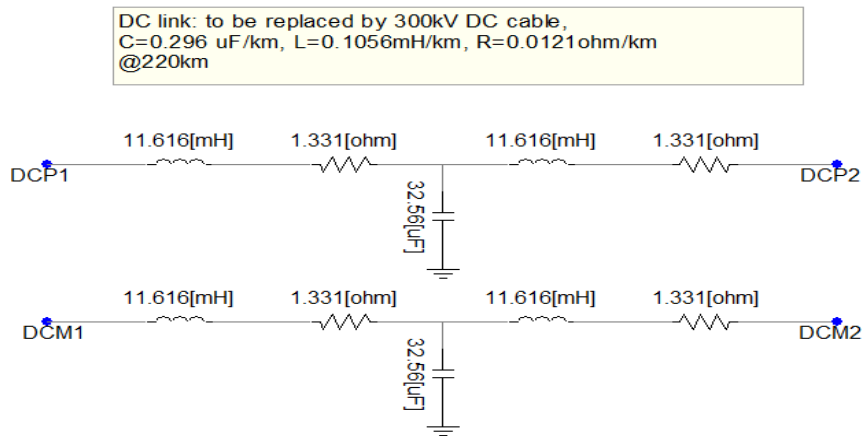


Figure 31 Equivalent circuit of dc model

[Screen shot from PSCAD program]

CHAPTER 5

INFLUENCE OF EMBEDDED HVDC ON SYSTEM PERFORMANCE

HVDC transmission links in parallel with AC lines are recommended to improve transient and dynamic stability as well as to damp over oscillations in power system [33].

The flexible AC transmission system (FACTS) concepts, which are in the basis of utilizing state-of-art power electronic technology with existing ac transmission system, are capable of improving system stability. Nonetheless paralleled operation of AC and VSC-HVDC transmission exerts superior characteristics in power system stability and security. The proposed power control methods are able to further improve the system dynamic performance.

This chapter presents a complete comparison among: AC transmission, embedded HVDC links, and embedded HVDC equipped with proposed power oscillation control scheme. In order to examine the capability of embedded HVDC transmission, several comparison groups for AC-DC parallel operation is to be described in this chapter. Therefore, before the test for the paralleled AC-DC transmission, the system with AC alone has been examined.

5.1 Critical Mode Test

The objective of critical mode test is to determine the maximum fault time at a fixed power flow. During the specific test, the tie-line flow is fixed at 300MW, and applying a three phase line to ground fault at middle of lines and at buses respectively.

The critical mode tests are conducted by Transient Stability Analysis Tool (TSAT) program, by using critical clearing time (CCT) calculation function. The CCT search threshold is set to 0.1 cycles.

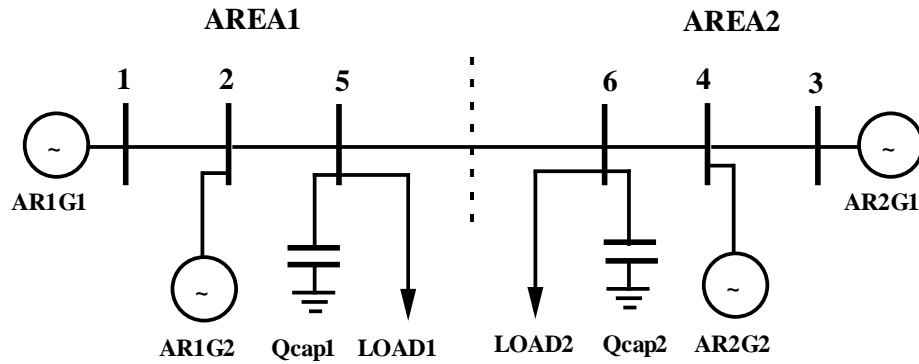


Figure 32A scheme of 6-bus 4-machine system

As shown in figure 32, the sample system is divided into two areas, that the bus 1, 2, and 5 are categorized to area 1, meanwhile that the bus 3, 4, and 6 are sorted into area 2.

5.1.1 Three phase line to ground fault at lines.

A typical contingency on these cases are setting as following illustrating:

At Time 2 Seconds

Three Phase Fault On Line ;1 ; 2 ; 1 50

(Note: Fault happens at the line between bus 1 and bus 2. The exact location is 50% of the line from bus 1.)

After 5.9 Cycles

Clear Three Phase Fault at Remote End

Clear Three Phase Fault at Near End

After 1 Cycles

Reconnect Line ;1 ; 2 ; 1

(Note: Reconnect the line between bus 1 and bus 2. The reconnection point is located at bus 1.)

5.1.2 Three phase line to ground fault on buses

A typical contingency on these cases are setting as following illustrating:

At Time 2 Seconds

Three Phase Fault at Bus ; 1

After 5.5 Cycles

Clear Three Phase Fault

5.1.3 Critical mode test result

Applying three phase line to ground fault on every case respectively, and the critical clearing time calculation result is listed on the Table 5 and 6. The test result graphs are shown in Appendix A.

Table 5 Line fault critical mode test result with HVAC transmission

Fault at Middle of Lines	Critical Clearing Time (cycles after fault)
Form Bus 1 to Bus 2	5.9
Form Bus 2 to Bus 5	4.9
Form Bus 3 to Bus 4	10.0
Form Bus 4 to Bus 6	11.3
Form Bus 5 to Bus 6	30.2

Table 6 Bus fault critical mode test result with HVAC transmission

Fault at Bus	Critical Clearing Time (cycles after fault)
Bus 1	6.3
Bus 2	5.2
Bus 3	10.0
Bus 4	11.3
Bus 5	6.2
Bus 6	12.9

5.2 Transient Stability Limit Test

The objective of transient stability test is to find out the maximum tie-line flow from area1 to area2 (the same as from bus 5 to bus 5), on condition of faults on different buses or lines with a fixed fault duration. In the following analysis, the fault clearing time

is fixed at 6 cycles and the tie-line flow is gradually increased till the stability limit reached.

The simulation programs on this stage are SSAT and PSAT, by employing functions of Stability Margin Calculation and Small-Signal Stability Limit Research. Meanwhile, a verification by program, PSCAD, on the same system has been conducted. Detailed simulation data has been attached in Appendix(a).

5.2.1 Fixed six cycles of three phase line to ground fault at buses

The typical contingency for fixed six cycles of three phase bus faults at buses is illustrated as following:

At Time 2 Seconds

Three Phase Fault at Bus ; 1

After 6.0 Cycles

Clear Three Phase Fault

The results are shown in 5.2.3.

5.2.2 Fixed six cycles of three phase line to ground fault at lines

The typical contingency for fixed six cycles of three phase line to ground faults at lines is illustrated as following:

At Time 2 Seconds

Three Phase Fault On Line ;1 ; 2 ; 1 50

After 6.0 Cycles

Clear Three Phase Fault at Remote End

Clear Three Phase Fault at Near End

After 1 Cycles

Reconnect Line ;1 ; 2 ; 1

5.2.3 Transient stability limit test results

By calculation the maximum power flow between area 1 and area 2, under the condition of a fixed six cycles of three phase line to ground fault at buses or lines respectively. The test results are shown in chapter 3 separately. Table 7 and Table 8 are the calculation results.

Table 7 Fixed line fault transient stability test result for the AC system

Fault on the Middle of Line	Maximum Tie-Line Flows (MW)
Between Bus 1 and Bus 2	295
Between Bus 2 and Bus 5	275
Between Bus 3 and Bus 4	370
Between Bus 4 and Bus 6	375
Between Bus 5 and Bus 6	414

Table 8 Fixed bus fault transient stability test result

Fault on Bus	Maximum Tie-Line Flows (MW)
Bus 1	309
Bus 2	304
Bus 3	371
Bus 4	280
Bus 5	305
Bus 6	383

From the table 5-8, the weakest bus is bus 2 and the highest risk of faults on transmission lines is the line between bus 2 and bus 5. Appendix (a) depicts the detailed simulation results, appendix (b) shows the power flow data used in the simulation and appendix (c) exhibits the dynamic data used in the system.

In the following analysis, dynamic performance comparisons among the HVAC transmission, embedded HVDC transmission and embedded HVDC transmission with designed controller will be described.

5.3 *Dynamic performance analysis*

5.3.1 *Stability performance comparison*

In this chapter, three cases have been performed to demonstrate system transient stability. On the basis of the conclusions from Section 5.2, a critical transmission power at 350MW is selected to test the system. The case A describes the connection between

area 1 and 2 is a HVAC transmission, while HVDC is not connected. In caseB, the connection between the two areas is a 200MW HVAC, and a 150MW VSC-HVDC. In case C, the connection between two areas is a 200MW HVAC, and a 150MW HVDC with power oscillation control as described in Chapter 4.

In the following analysis, several cases have been depicted respectively.

Case A The transmission between two areas is a 350 MW AC, but DC line is not connected

By placing a three-phase line-to-ground fault at four typical buses on the system, the critical clearing time of each case can be calculated. The Critical Clearing Time is the maximum time during which a disturbance can be applied without the system losing its stability.

Table 9 illustrates the critical clearing time at each bus when tie line flow is 350 MW HVAC transmission only.

Table 9 Critical clearing time at each bus when tie line flow is 350MW HVAC

Three phase line-to-ground fault	Critical Clearing Time (ms)
Bus 2	100
Bus 4	210
Bus 5	90
Bus 6	180

Based on Table 9, the critical clearing time on the four buses ranges from 90ms to 210ms, therefore a conclusion can be determined that the weakest bus on the system is the bus 5 with a critical clearing time of 90ms under a three-phase line-to-ground fault.

Consequently, placing a 100ms line-to-ground fault at bus 5 is expected to result a system instability. In order to ensure the conclusion above.

The relative phase angles of the generators are shown in Figure 33. Figure 33 describes the relative phase angles of the generator with a time range from 1.0 second to 6.0 second.

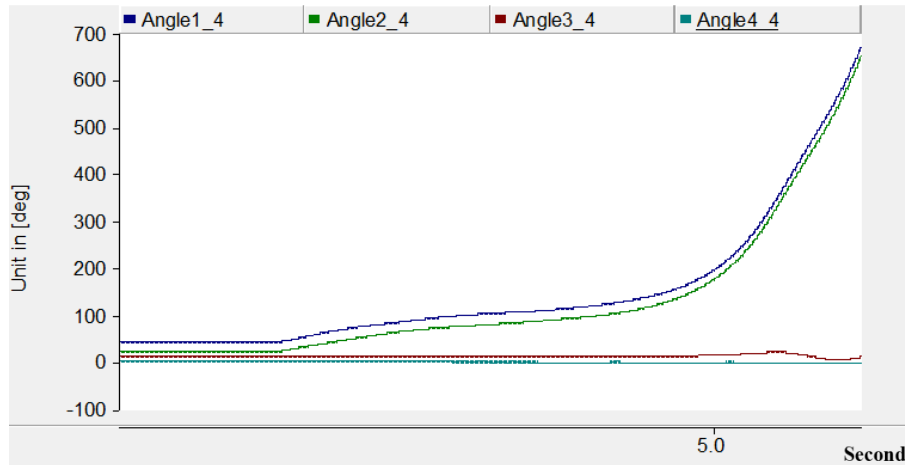


Figure 33 Relative phase angles of generators

According to Figure 33, by placing a 100ms three-phase line-to-ground fault at bus 5, the phase angles of each generator are not following each other, hence, the system is insecure.

Case B The transmission between two areas is 200 MW AC paralleled with 150 MW classical VSC-HVDC

In this case, a conventional d-q vector control methods are employed on VSC-HVDC. HVDC transmission is working simultaneously with HVAC. By applying a three-phase line-to-ground fault on bus 5 with the same time duration of 100ms, the phase angle of each generator have been determined. Figure 34 shows the relative phase angle of each generator under the influence of the proposed fault.

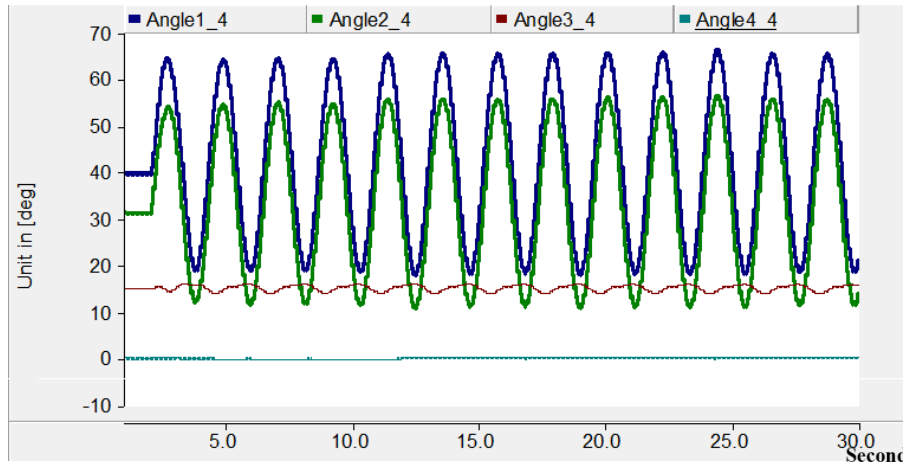


Figure 34 Relative phase angle of each generator

According to Figure 34, the phase angles are not following each other. However, the system dynamic performance is more stable than Case A.

Case C The transmission between two areas is 200 MW AC paralleled with 150 MW VSC-HVDC by proposed control method

In this case, a power oscillatory loop controller is applied on the HVDC active power reference to compensate the oscillation. In order to test the system dynamic performance, a 100 ms three phase line to ground fault is applied at bus 5, the weakest bus in the system.

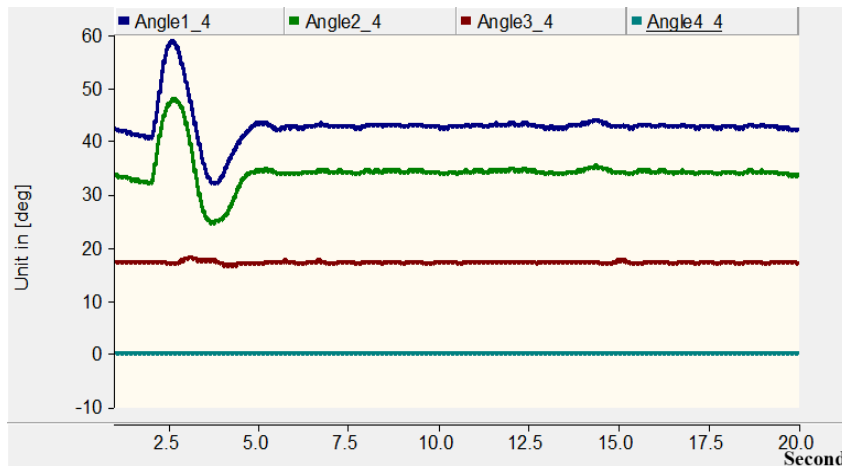


Figure 35 Relative phase angle at each generator

Figure 36 shows the relative phase angles at each generator terminal. From the diagram, the system is secure and more stable than the system in case B. Figure 37 shows the compensation power supplied from power control loop, which compensates the power oscillation from area 1 to area 2.

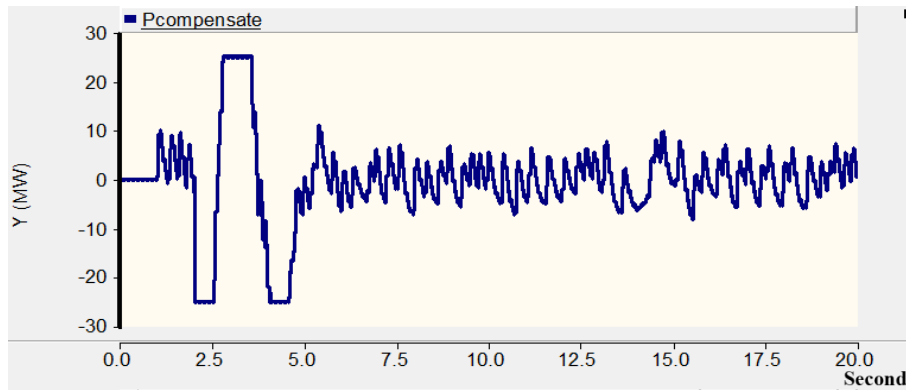


Figure 36 The compensation power supplied from power control loop

Then increase the three phase line-to-ground fault duration to 360ms, the relative phase angle, terminal voltage and power flow with 360ms fault is shown in the following figures. From the figures, the system is still stable at this case. When continue to increase the fault duration to 370ms, the system becomes insecure. Therefore, the critical clearing time with a three phase line-to-ground fault at bus 5 is 360ms.

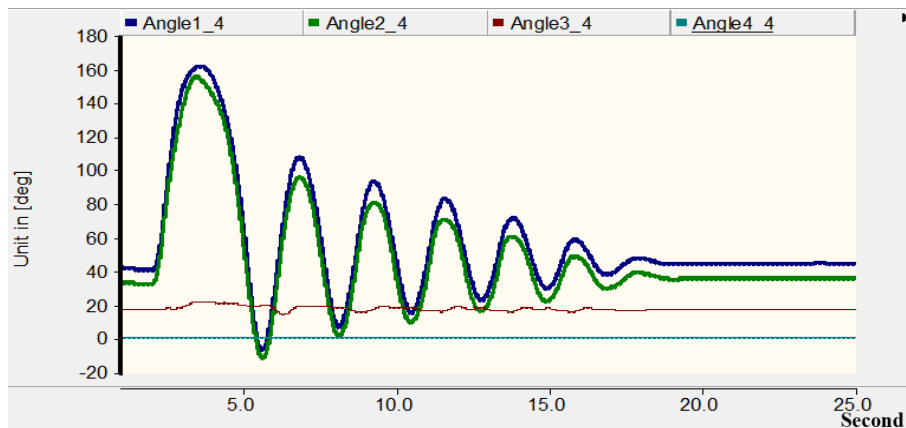


Figure 37 Relative phase angle of each generator

Figure 38 shows the relative phase angle of each generator, and figure 39 shows the compensation power provided from power control loop while the system has a critical fault duration of 360ms.

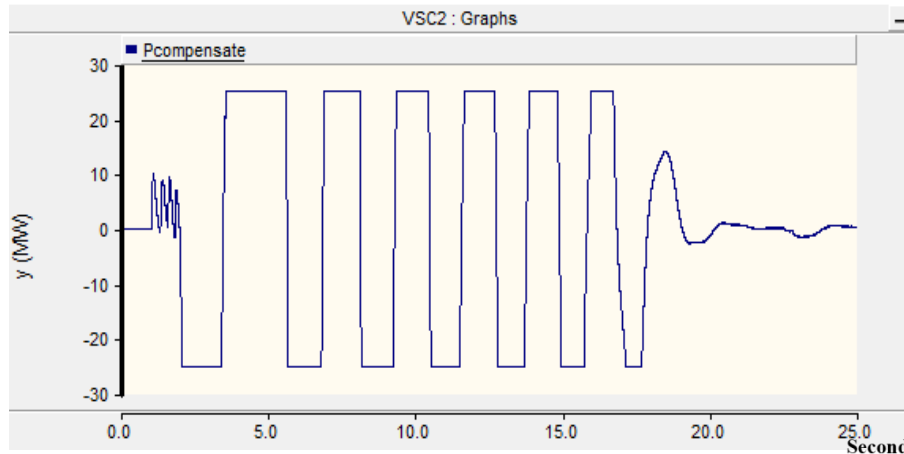


Figure 38 The compensation power supplied from power control loop

From the cases above, the system with 200MW HVAC and 150MW HVDC with power control is the most stable one. Therefore, the system stability has been highly improved by the power control loop.

According to the test results above, the VSC-HVDC paralleled operation with traditional HVAC system exerts a better dynamic performance than HVAC transmission system alone. Nevertheless, the proposed control mechanism, by employing the angular frequency difference from two VSC station ac terminals as the input reference, further improves the dynamic performance as well as the stability and security of the whole system.

CHAPTER 6

CONCLUSIONS AND PROSPECTS

In spite of the constantly growing number of HVDC schemes worldwide, those which comply to the definition of embedded HVDC in an AC system are more limited. Yet, the survey of existing and planned embedded HVDC exhibits several drivers which may lead to prefer this hybrid solution over more classical alternatives. In addition to usual rationale for HVDC, other possible grounds are the ability to control power flow or the delivery of ancillary services.

Embedded HVDC, like FACTS, are active equipments which provide supplementary control over the AC network in which they are installed. This gain in flexibility comes at the expense of complexity. Depending on the underlying DC technology, different technical issues arise, along with different features and performances. Hence, each project leads to different choices, such as: static power dispatch on hybrid AC/DC transmission corridors; design of an automatic system security control; Contribution to voltage or reactive support; system stability enhancement for transient stability and recovery; power oscillation damping; supplementary controls activated under specific conditions; etc.

Most of the corresponding features and requirements have a large impact on the solution that manufacturers can provide, while others are to a certain extent independent from the HVDC technology such as AC and DC power flow optimization and frequency control.

This thesis provides a benchmark network model which can be fully implemented in any appropriate tool and used to perform studies on the hybrid AC/DC systems to

illustrate the overall performance during and after contingencies. Also, the thesis proposes a control scheme for embedded HVDC system to further limit active power oscillation and regulate the dc voltage.

The wide range of features provided by HVDC links requires additional attention for its integration into an AC network with others existing equipments. Moreover, the operation of such a device with regards to other HVDC, FACTS or PST requires a global view that certainly goes beyond the usual operation of power transmission systems. Thus, the insertion of an HVDC link into an AC system appears both with different coordination needs (at the local, national, and trans-national levels), and with different constraints depending on the integration process (at the planning phase, during the testing and early operations, or under exploitation).

REFERENCES

- [1] N. Flourentzou, Vassilios G. Agelidis, Georgios D. Demetriades, "VSC-Based HVDC Power Transmission Systems: An Overview" IEEE Transactions on Power Electronics, vol. 24, no. 3, pp 592-602 Mar. 2009.
- [2] B. Andersen and C. Barker, "A new era in HVDC?" Inst. Elect. Eng.(IEE) Rev.,vol.46, no.2, pp 33-39, 2000.
- [3] W. Long and S. Nilsson, "HVDC transmission yesterday and today," IEEE Power Energy, vol.5, no.2, pp.22-31, Mar. /Apr. 2007.
- [4] S. Henry, O.Despouys, and G. Karady, "Influence of Embedded HVDC Transmission on System Security and AC Network Performance," Cigre Brochure JWG C4-B3-C1.604.
- [5] Roberto Rudervall, J.P. Charpentier, Raghuveer Sharma, "High Voltage Direct Current(HVDC) Transmission Systems Technology Review Paper," Energy Week, Mar 2000
- [6] Jenny Paulinder, "Operation and control of HVDC links embedded in AC system," Thesis for the degree of licentiate of engineering, Chalmers University of Technology, Goteborg, Sweden, 2003
- [7] P. Kundur, "Power system stability and control," ISBN 0-07-035958-X, McGraw-Hill, 1994.
- [8] "IEEE guide for planning DC links terminating at AC locations having low short-circuit capacities," IEEE Std1204-1997, Tech. Rep., 1997.
- [9] L. Zhang and L. Dofnas, "A novel method to mitigate commutation failures in HVDC systems," in Power Conference 2002, Kunming, China, 2002.
- [10] "IEEE guide for planning DC links terminating at AC locations having low short-circuit capacities," IEEE Std1204-1997, Tech. Rep., 1997.
- [11] G. Asplund, K. Eriksson, and K. Svensson, "HVDC light-DC transmission based on voltage-sourced converter," Asea Brown Boveri Ltd. Rev., vol.1, pp. 4-9, 1998.
- [12] J. Rodriguez, J.S. Lai, and F. Z. Peng, "Multilevel interter: a survey of topologies, controls, and applications," IEEE Trans. Ind. Elect., vol. 49, no. 5, pp. 724-738, Aug. 2002
- [13] L. Zhang, L. Harnefors, and P. Rey, "Power system reliability and transfer capability improvement by VSCHVDC," Cigre Regional Meeting, Tallin, Estonia, 2007.

- [14] Jochen Kreusel, Dietmar Retzmann, "Integrated AC/DC Transmission Systems --- - Benefits of Power Electronics for Security and Sustainability of Power Supply," PSCC 2008, July 2008
- [15] M. P. Bahrman, "HVDC transmission overview," Proc. IEEE Power Energy Soc. Transmiss. Distrib. Conf. Expo., Chicago, IL, Apr. 21–24, pp. 1–7, 2008
- [16] Shuhui Li, "Control of HVDC light system using conventional and direct current vector control approaches," IEEE Transactions on Power Electronics, vol. 25, no. 12, pp 3106-3118, Dec. 2010
- [17] S. Li and T. A. Haskew, "Transient and steady-state simulation of decoupled d–q vector control in PWM converter of variable speed wind turbines," in Proc. 33rd Annu. Conf. IEEE Ind. Electron. (IECON 2007), Taipei, Taiwan, Nov. 5–8, pp. 2079–2086.
- [18] A. Yazdani and R. Iravani, "Dynamic model and control of the NPC based back-to-back HVDC system," IEEE Trans. Power Del., vol. 21, no. 1, pp. 414–424, Jan. 2006.
- [19] S. Ruan, G. Li, L. Peng, Y. Sun, and T. T. Lie, "A nonlinear control for enhancing HVDC light transmission system stability," Int. J. Electr.Power Energy Syst., vol. 29, pp. 565–570, 2007.
- [20] R. Gagnon, Detailed model of a doubly fed induction generator(DFIG) driven by a wind turbine. Natick, MA: The Math Work, Jan. 2006.
- [21] S. Casoria, VSC-based HVDC Transmission Link. Natick, MA: The Math Work, Jan, 2006.
- [22] T. G. Magg, H. D. Mutschler, S. Nyberg, J. Wasborg, H. Thunehed, B. Sandberg, "Caprivi link HVDC interconnector: site selection, geophysical investigations, interference impacts and design of the earth electrodes," CIGRE 21 rue d'Artois F-75008, Paris, 2010.
- [23] T. Shimato, T. Hashimoto, M. Sampei, "The Kii Channel HVDC link in Japan," CIGRE 21 rue d.Artois F-75008, Paris, 2002.
- [24] Hiroyuki Nakao, Masahiro Hirose, Takehisa Sakai, Naoki Kawamura, Hiroaki Miyata, Makoto Kadowaki, Takahiro Oomori, Akihiko Watanabe, "The 1,400-MW Kii-Channel HVDC System," Hitachi Review vol. 50, no.3, 2001
- [25] Electricity sector in Japan. [Online]. Available: http://en.wikipedia.org/wiki/Electricity_sector_in_Japan.TM T&D Corporation, "Kii Channel HVDC Link," Japan, 2000.

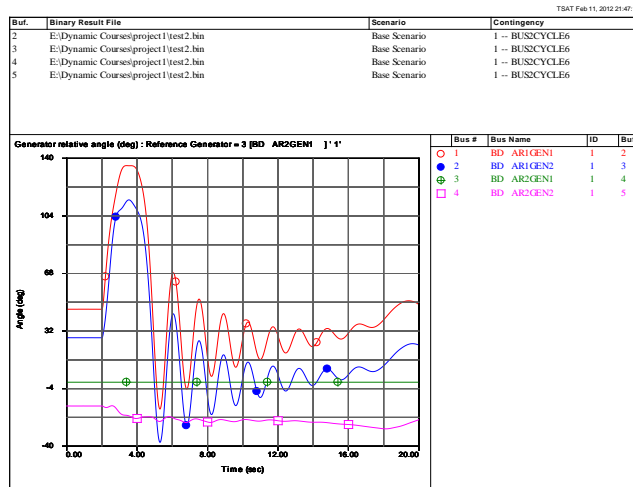
- [26] HVDC Kingsnorth. [Online]. Available: http://en.wikipedia.org/wiki/HVDC_Kingsnorth.
- [27] R. Yacamini, "Instability in h.v.d.c. schemes at low-order integer harmonics," IEE PROC. vol. 127, Pt. C, no. 3, May 1980.
- [28] T. Rauhala, J. Jyrinsalo, H. Kuisti. "Enhancing the transmission capability using FACTS: the Finnish Experience" in IET AC and DC Transmission system conference, London, UK, 2010.
- [29] "Development of electricity supply to the NSW far north coast," [Online]. Available: <http://www.transgrid.com.au/network/consultations/Documents/110208%20%20Far%20North%20NSW%20%20Supplementary%20Report%20Final.pdf>
- [30] Terranora interconnector (Directlink). [Online]. Available: <http://www.abb.us/industries/ap/db0003db004333/2700978c26a07a70c125774b00410cbc.aspx>
- [31] Dirk Van Hertem, Jody Verboomen, Stijn Cole, Wil Kling, Ronnie Belmans, "Influence of phase shifting transformers and HVDC on power system losses,"
- [32] T. Vijay Muni, T. Vinoditha, D. Kumar Swamy, "Improvement of Power System stability by Simultaneous AC-DC Power Transmission," International Journal of Scientific & Engineering Research, vol. 2, issue 4, April 2011.
- [33] Lidong Zhang <lidong.zhang@se.abb.com>, ABB.

APPENDIX A
DYNAMIC PERFORMANCE DIAGRAMS

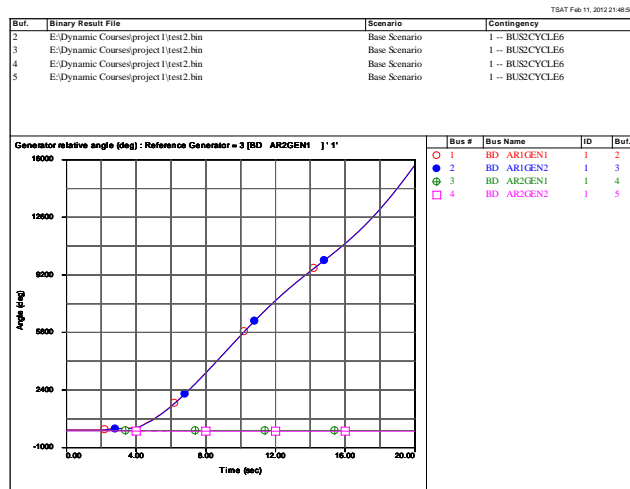
A) Critical Mode Test

I. Three Phase Line to Ground Fault at Lines of Middle of Buses

- o Fault at middle of line between bus 1 and 2.

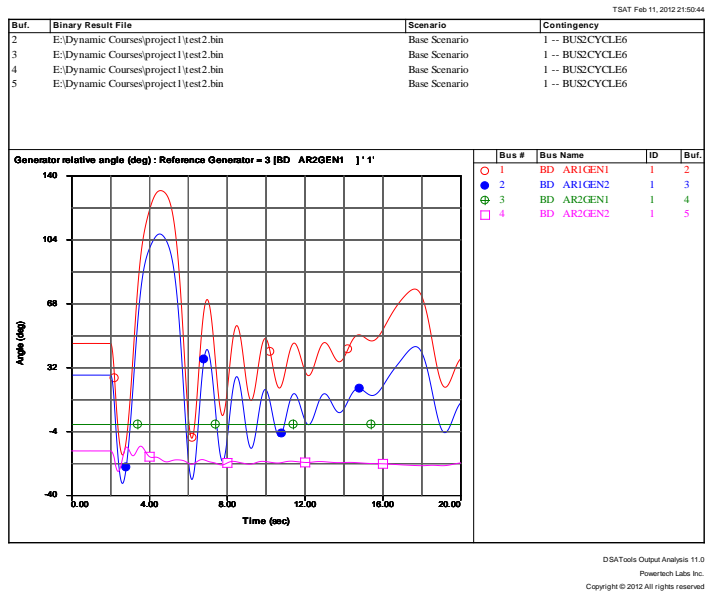


Generator phase angles when fault clears at 5.9 cycles (stable)

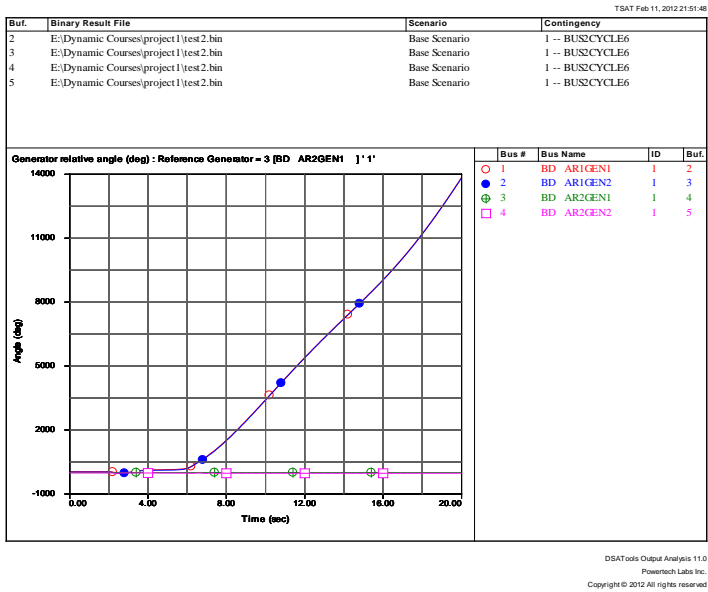


Generator phase angles when fault clears at 6.0 cycles (unstable)

- Fault at middle of line between bus 2 and 5.

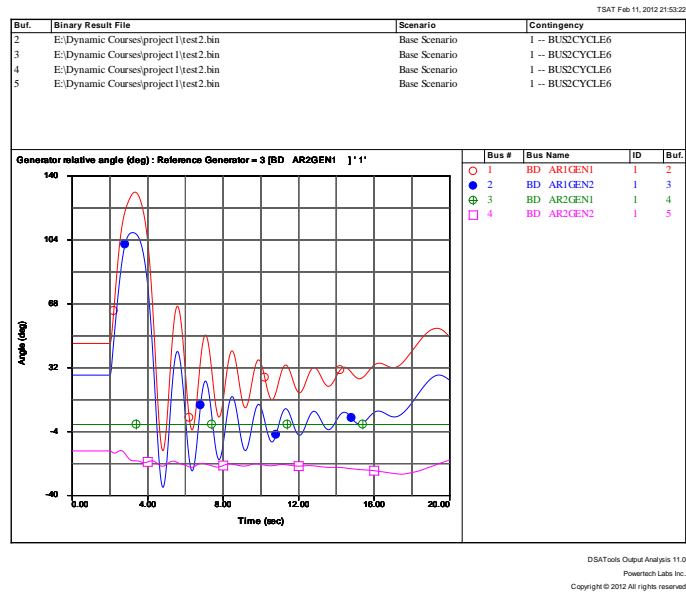


Generator phase angles when fault clears at 10.0 cycles (stable)

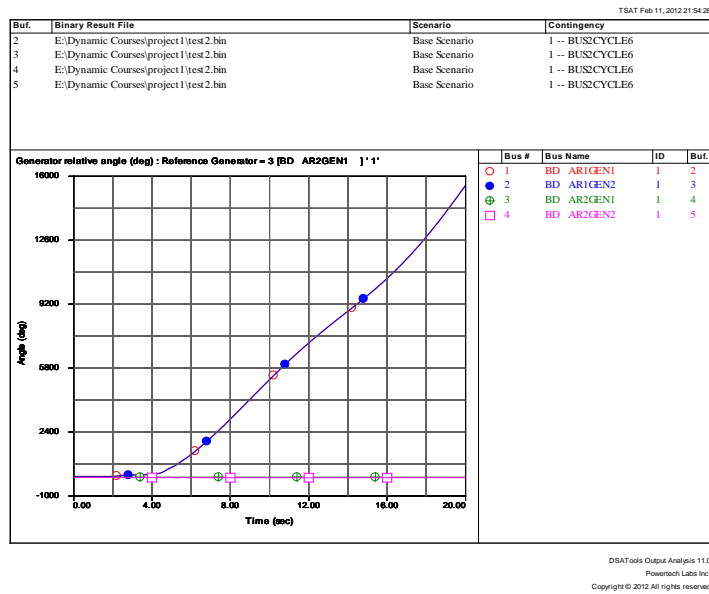


Generator phase angles when fault clears at 10.1 cycles (unstable)

- Fault at middle of line between bus 2 and 5.

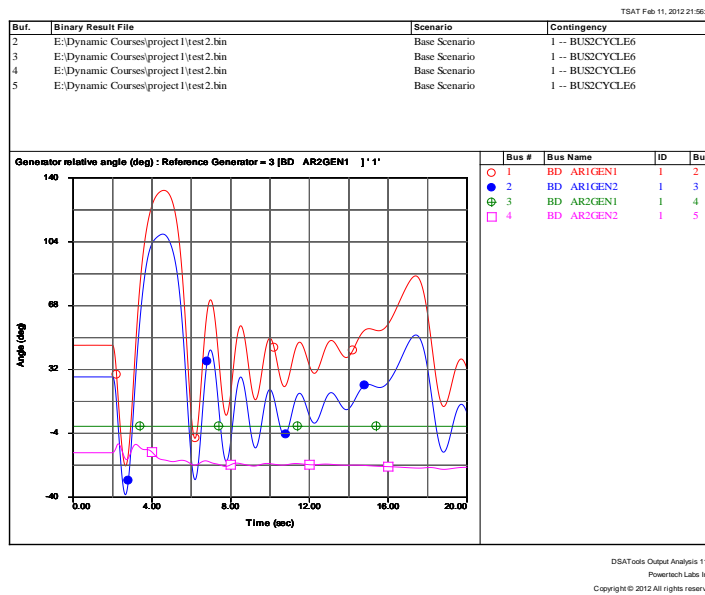


Generator phase angles when fault clears at 4.9 cycles (stable)

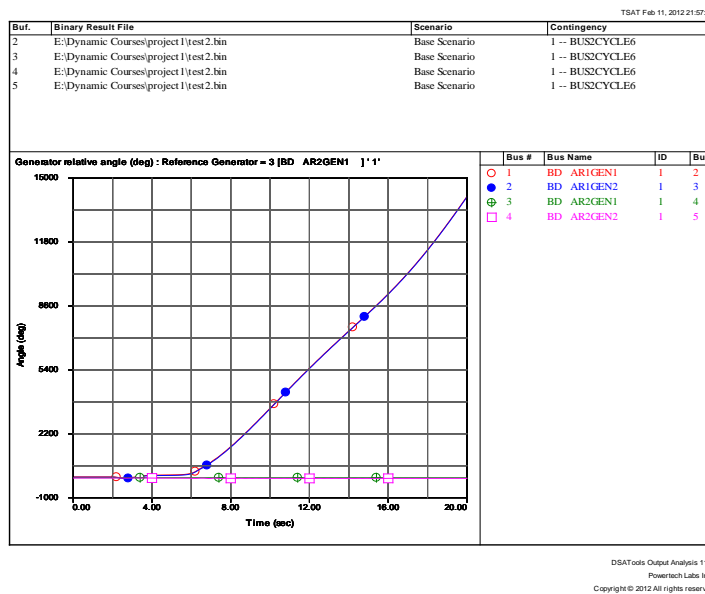


Generator phase angles when fault clears at 5.0 cycles (unstable)

- Fault at middle of line between bus 4 and 6.

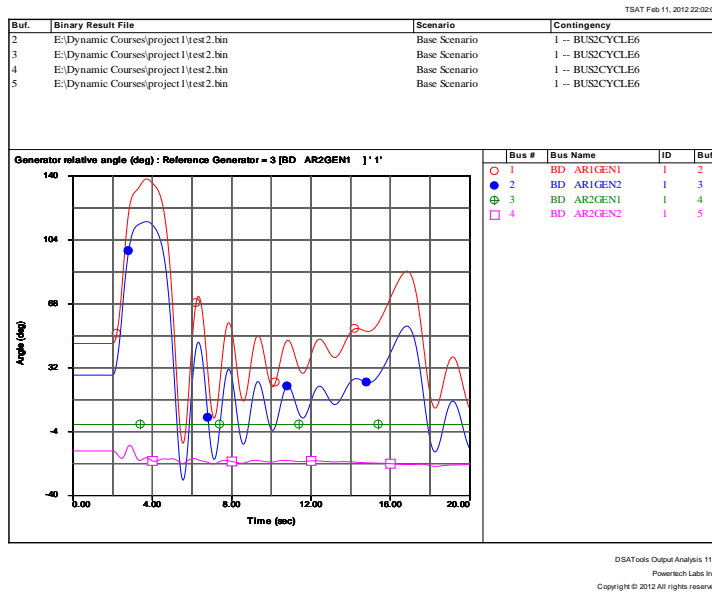


Generator phase angles when fault clears at 11.3 cycles (stable)

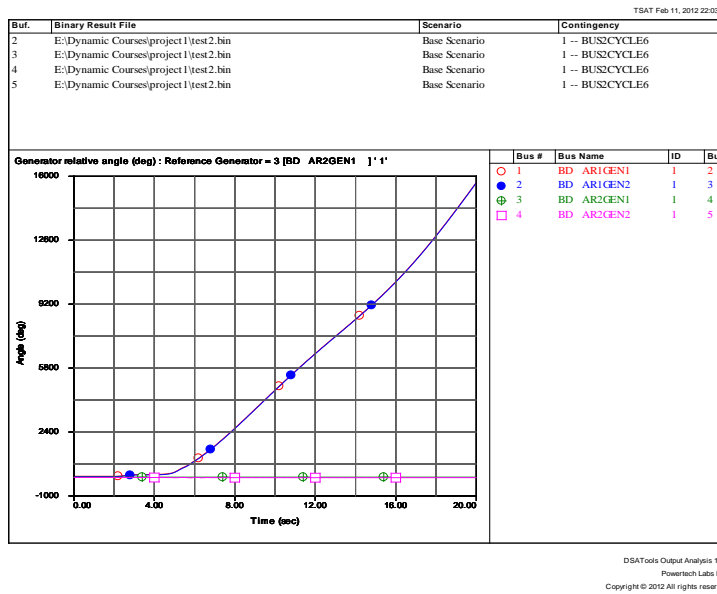


Generator phase angles when fault clears at 11.4 cycles (unstable)

- Fault at middle of line between bus 5 and 6.



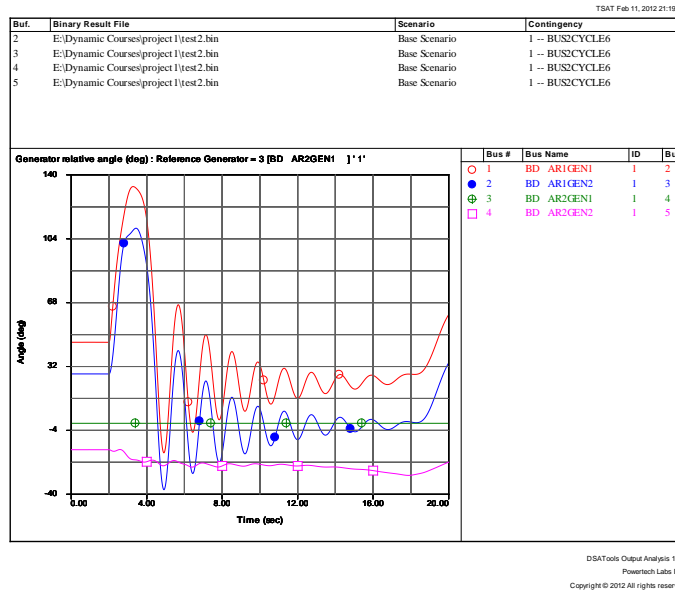
Generator phase angles when fault clears at 30.2 cycles (stable)



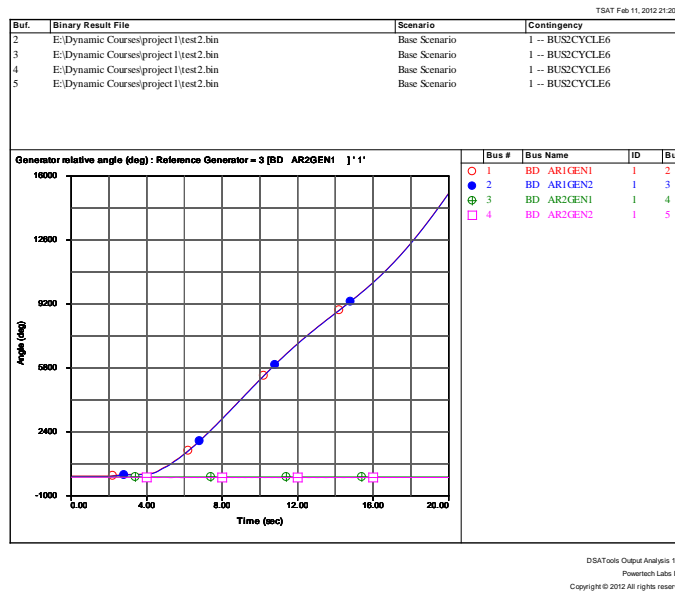
Generator phase angles when fault clears at 30.3 cycles (unstable)

II. Three phase line to ground fault at buses.

- Fault at bus 1.

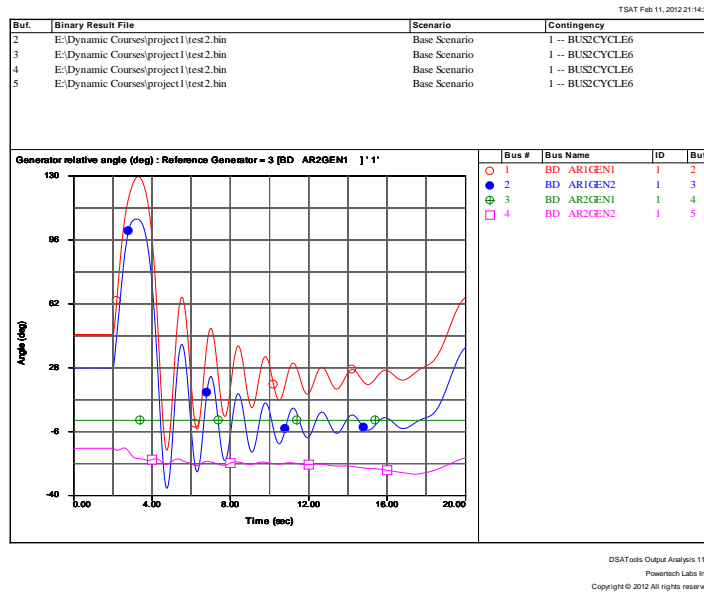


Generator phase angles when fault clears at 6.3 cycles (stable)

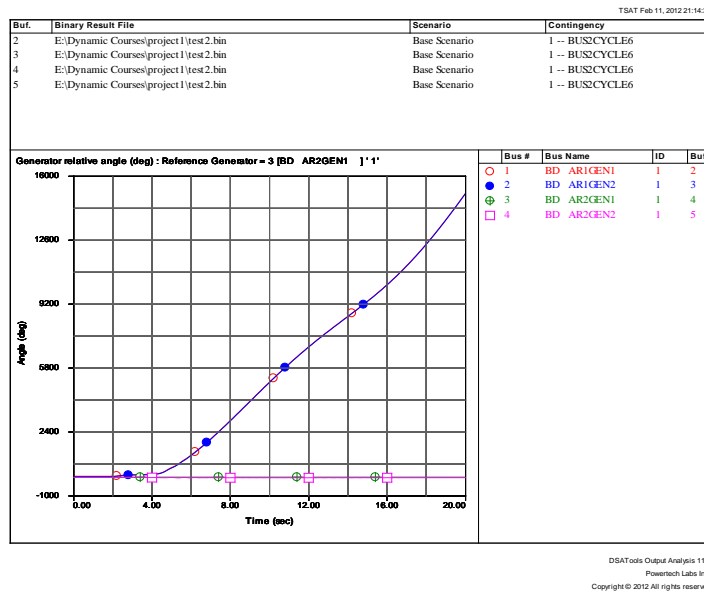


Generator phase angles when fault clears at 6.4 cycles (unstable)

- Fault at bus 2.

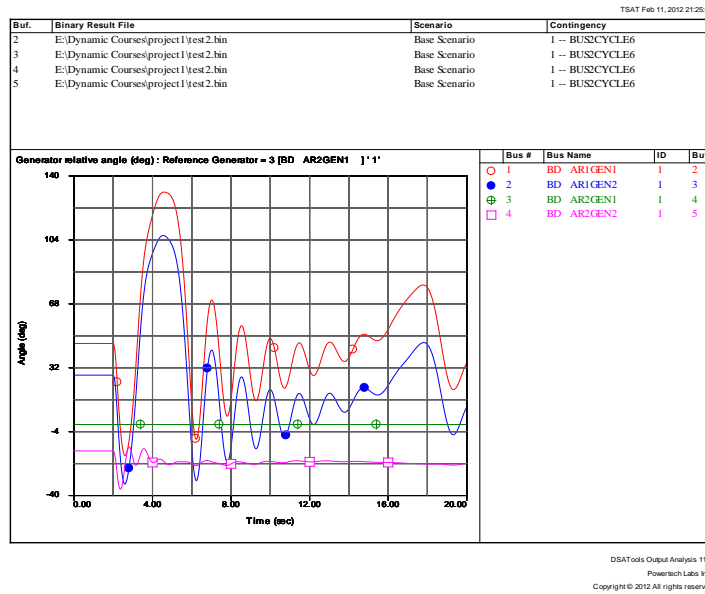


Generator phase angles when fault clears at 5.2 cycles (stable)

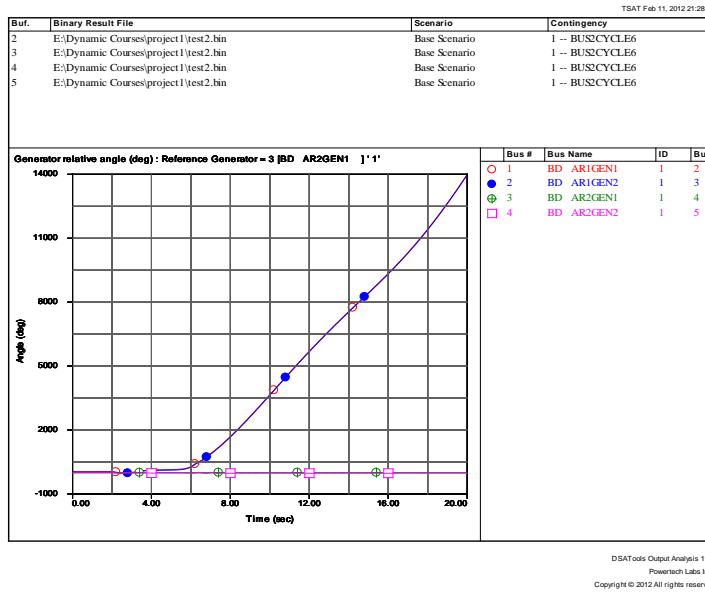


Generator phase angles when fault clears at 5.3 cycles (unstable)

- Fault at bus 3.

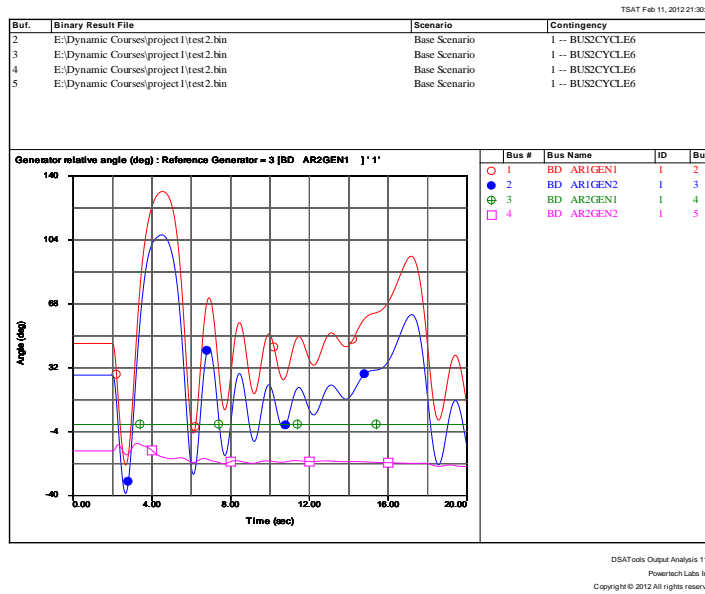


Generator phase angles when fault clears at 10.0 cycles (stable)

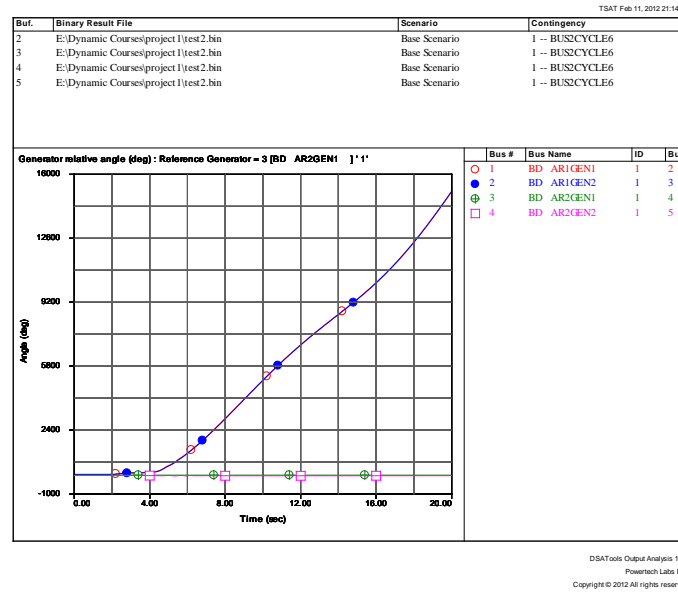


Generator phase angles when fault clears at 10.1 cycles (unstable)

- Fault at bus 4.

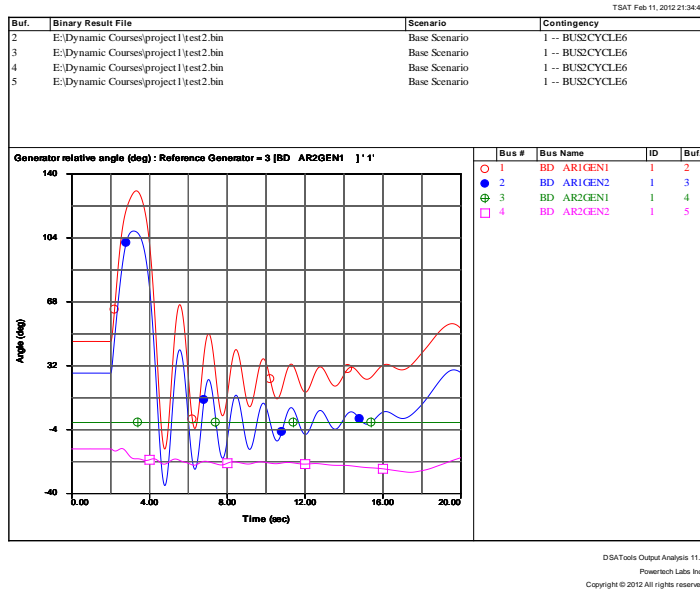


Generator phase angles when fault clears at 11.3 cycles (stable)

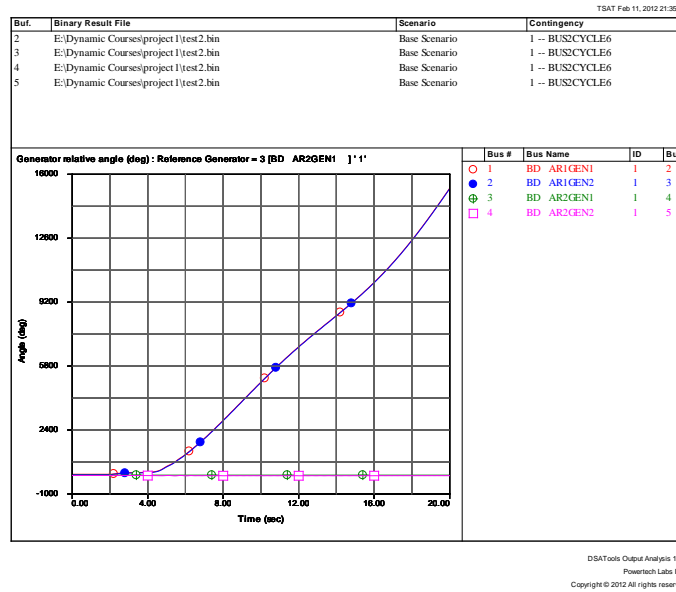


Generator phase angles when fault clears at 11.4 cycles (unstable)

- Fault at bus 5.

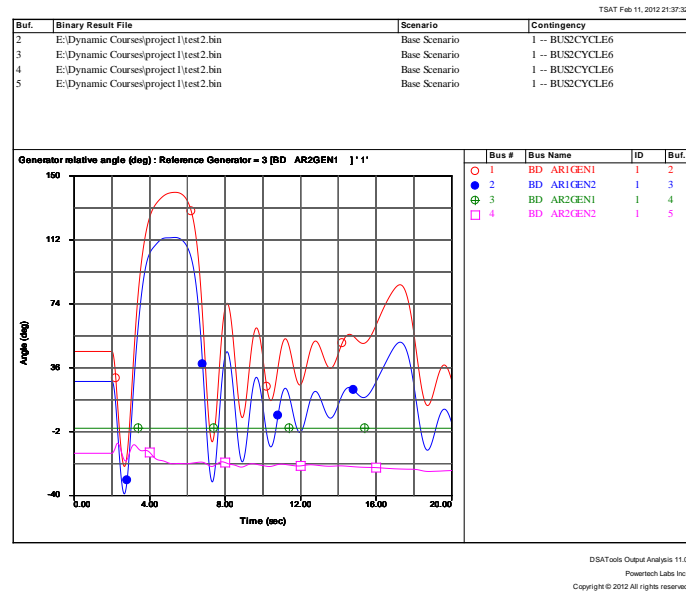


Generator phase angles when fault clears at 5.2 cycles (stable)

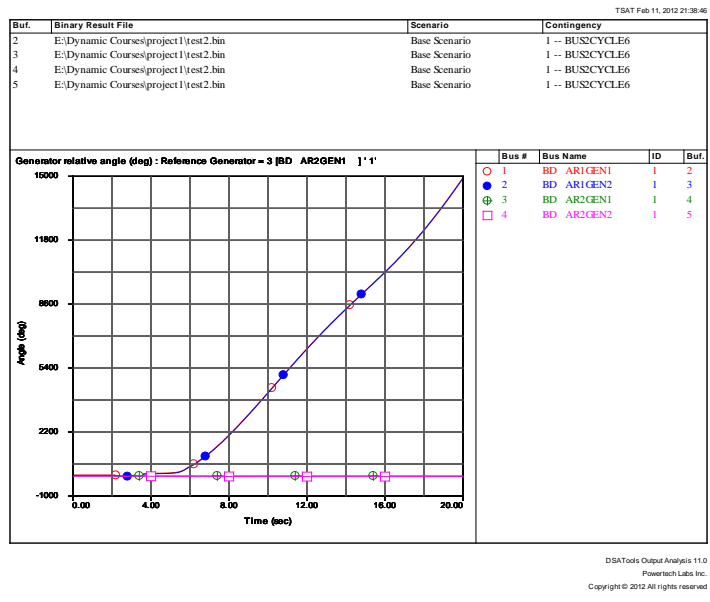


Generator phase angles when fault clears at 5.3 cycles (unstable)

- Fault at bus 6.



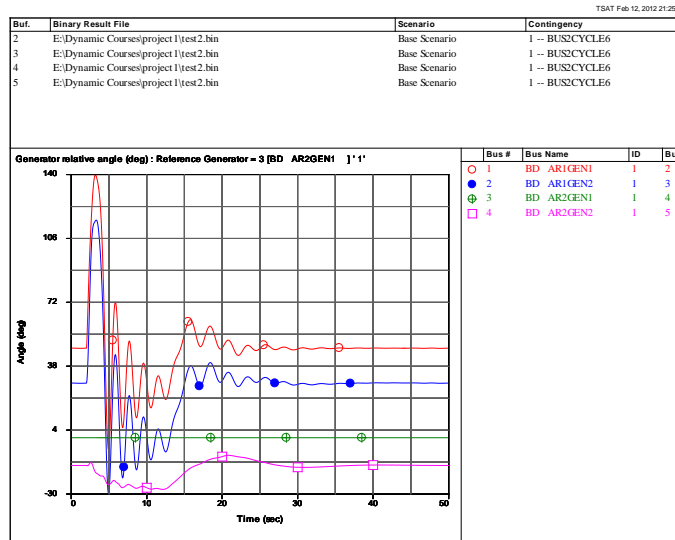
Generator phase angles when fault clears at 12.9 cycles (stable)



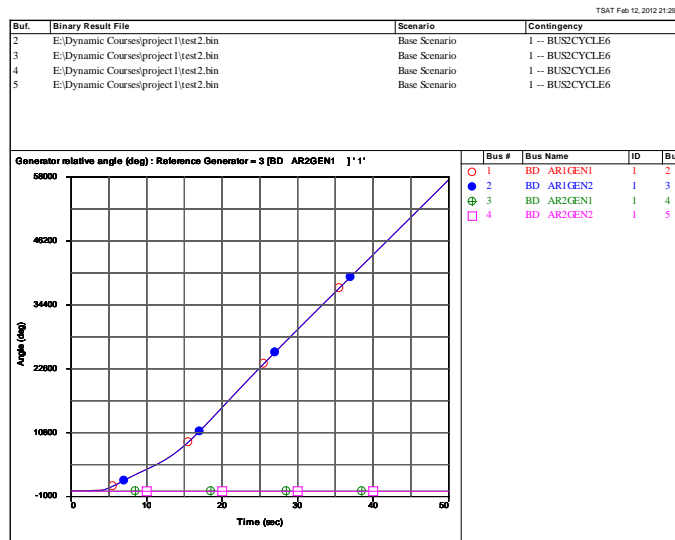
Generator phase angles when fault clears at 13.0 cycles (unstable)

B) Transient Stability Limit Test

- I. Fixed Six Cycles of Three Phase line to Ground fault at buses
 - o Fault at bus 1

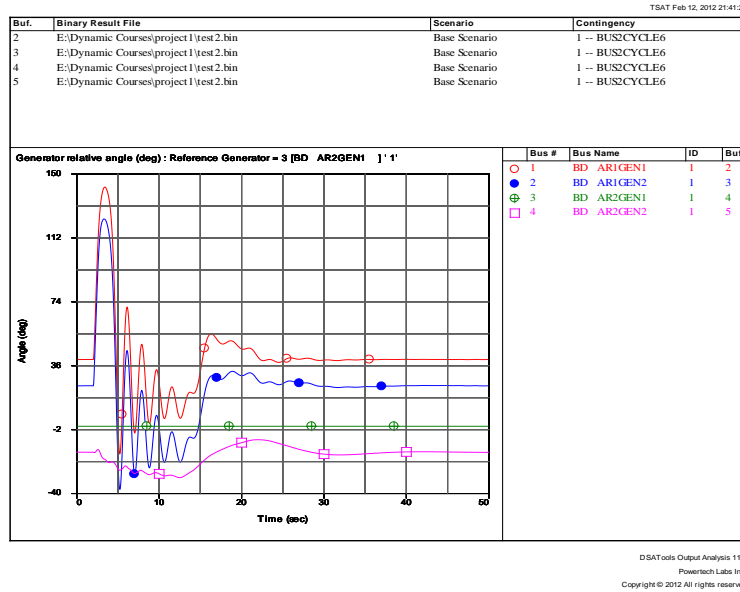


Generator phase angles when tie-line flow is 309 MW (stable)

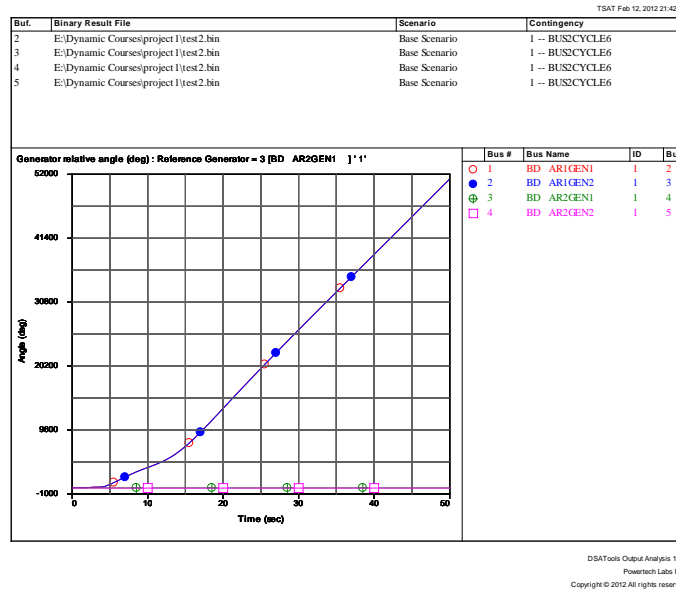


Generator phase angles when tie-line flow is 310 MW (unstable)

○ Fault at bus 2

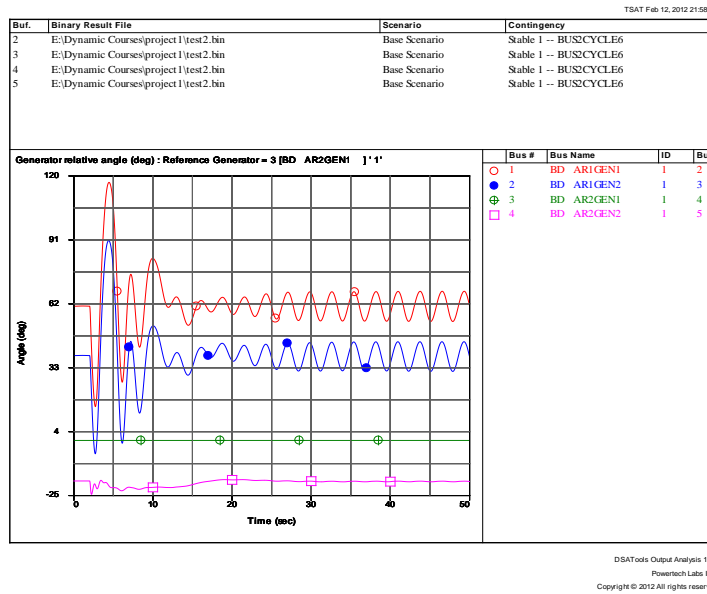


Generator phase angles when tie-line flow is 279 MW (stable)



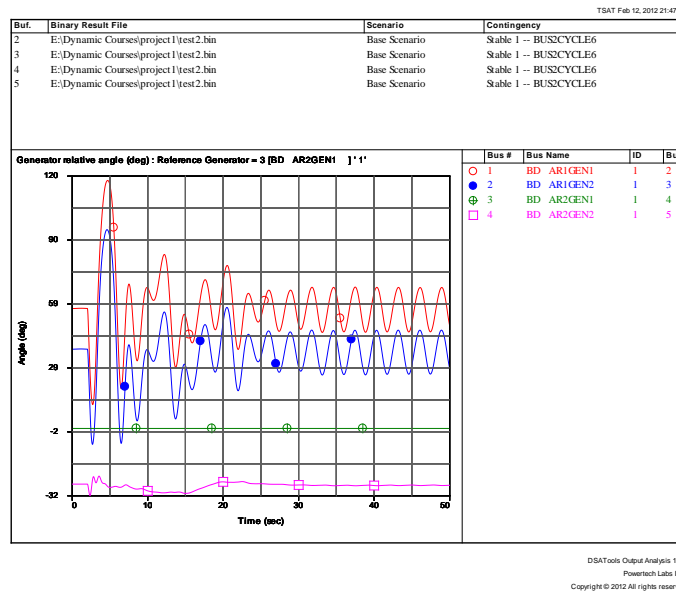
Generator phase angles when tie-line flow is 280 MW (stable)

○ Fault at bus 3



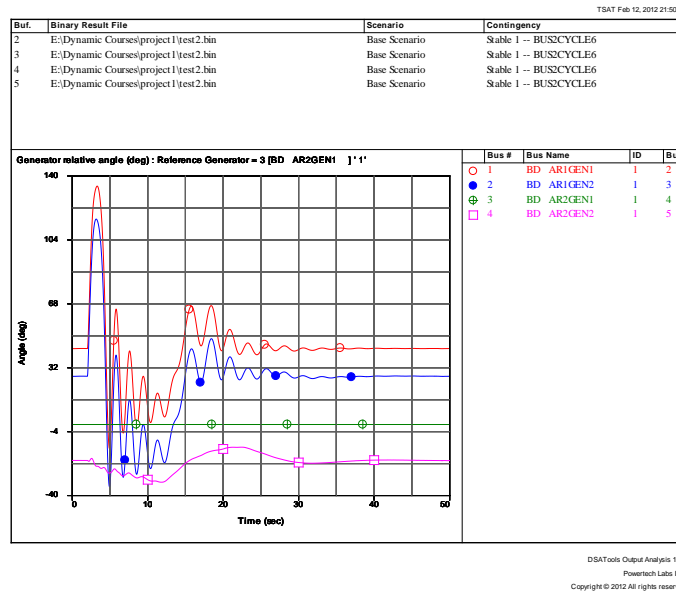
Generator phase angles when tie-line flow is 371 MW (stable)

○ Fault at bus 4



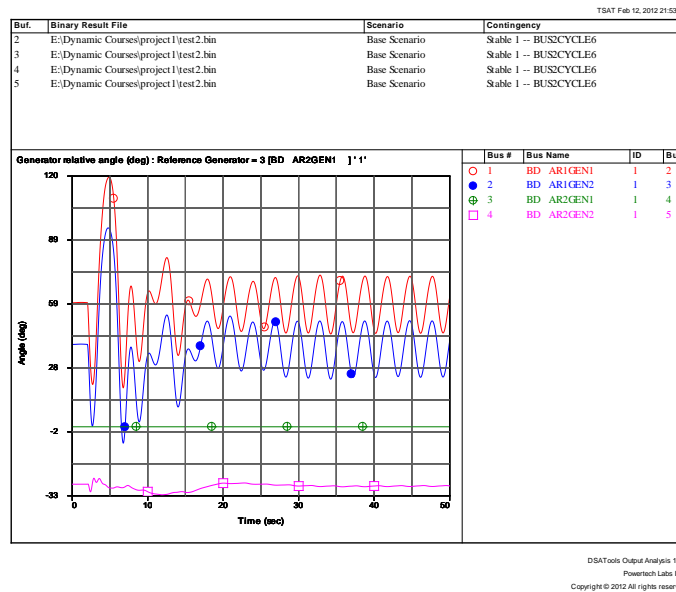
Generator phase angles when tie-line flow is 274 MW (stable)

- Fault at bus 5



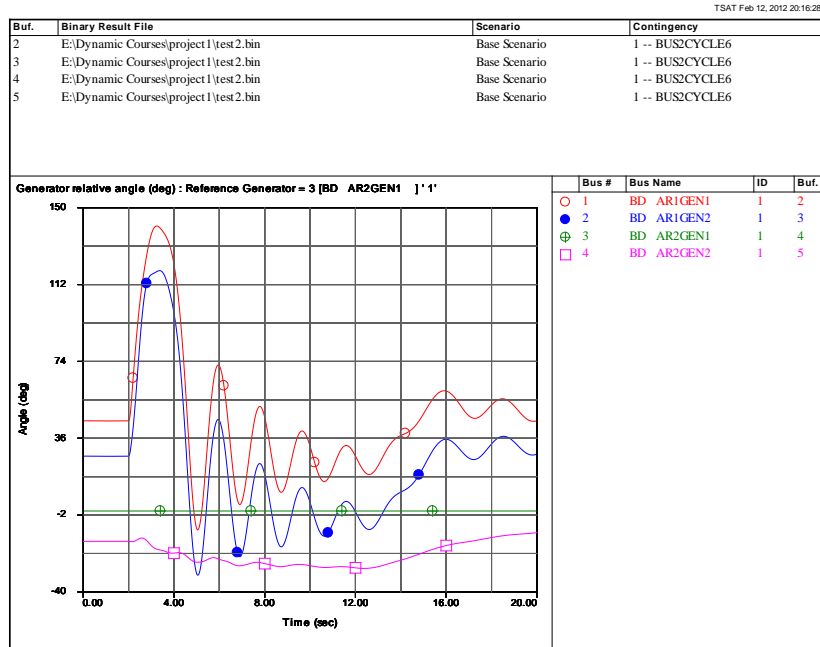
Generator phase angles when tie-line flow is 305 MW (stable)

- Fault at bus 6



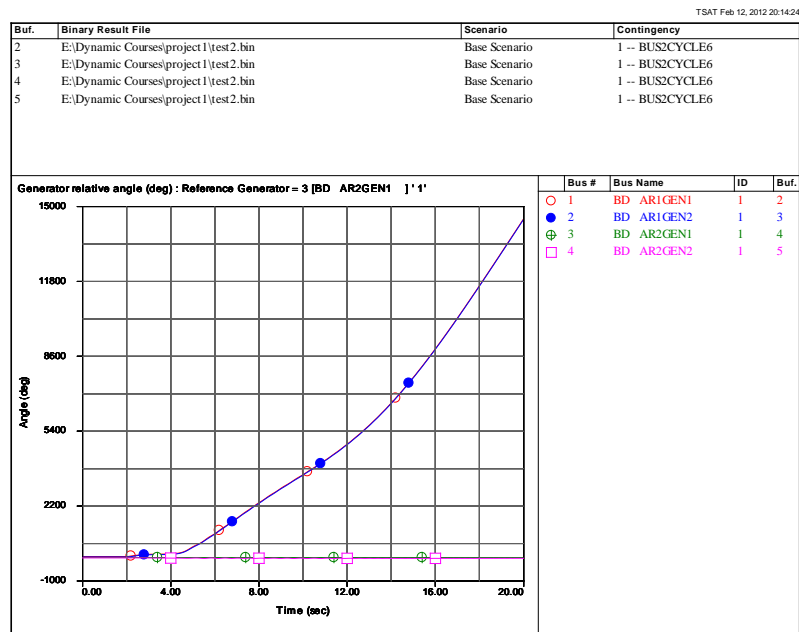
Generator phase angles when tie-line flow is 383 MW (stable)

II. Fixed six cycles of three phase line to ground fault at lines of middle of buses
 ○ Fault at middle of lines between bus 1 and 2



DSATools Output Analysis 11.0
 Powertech Labs Inc.
 Copyright © 2012 All rights reserved

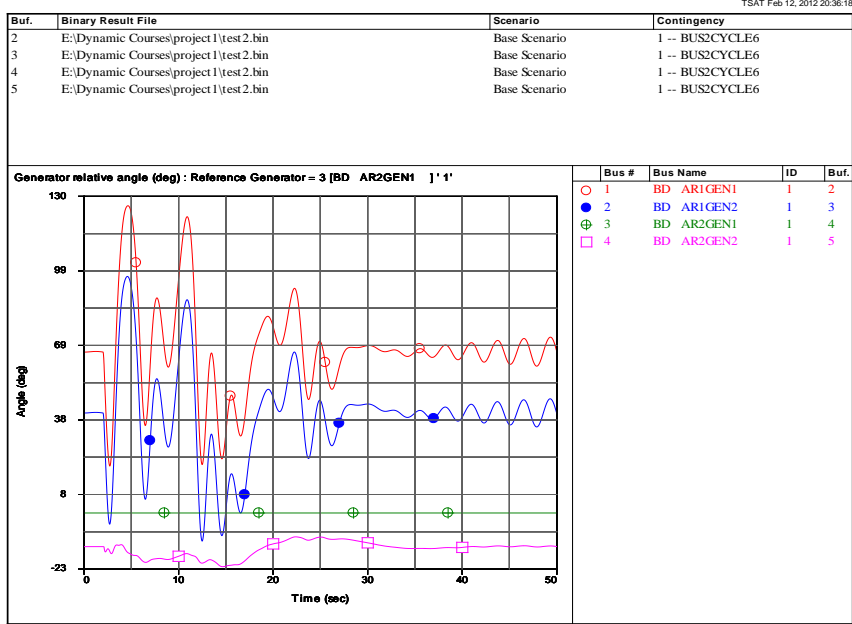
Generator phase angles when tie-line flow is 295 MW (stable)



DSATools Output Analysis 11.0
 Powertech Labs Inc.
 Copyright © 2012 All rights reserved

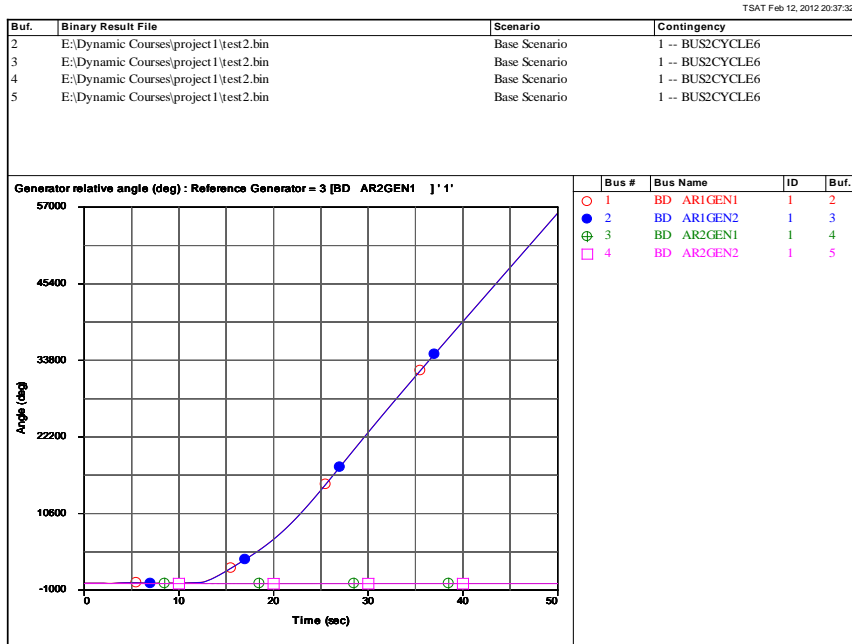
Generator phase angles when tie-line flow is 296 MW (unstable)

- Fault at middle of lines between bus 3 and 4



DSATools Output Analysis 11.0
Powertech Labs Inc.
Copyright © 2012 All rights reserved

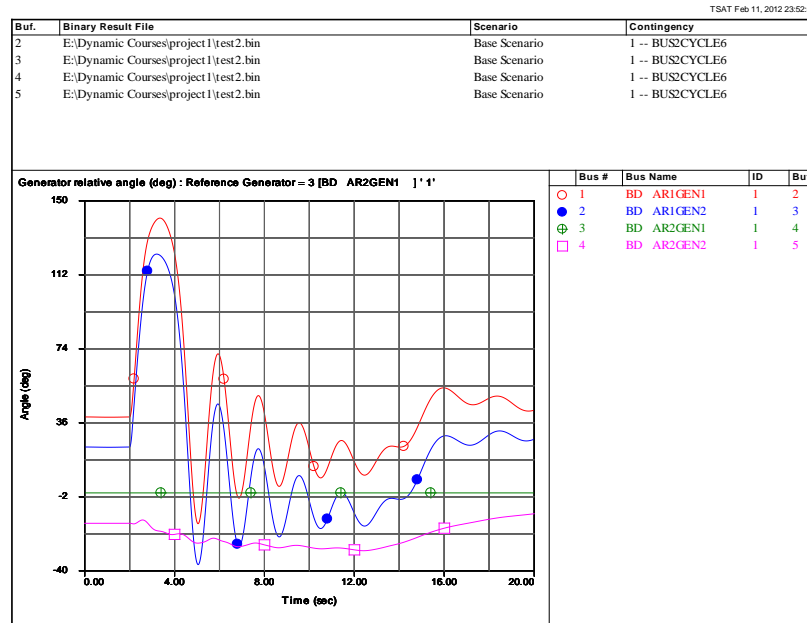
Generator phase angles when tie-line flow is 370 MW (stable)



DSATools Output Analysis 11.0
Powertech Labs Inc.
Copyright © 2012 All rights reserved

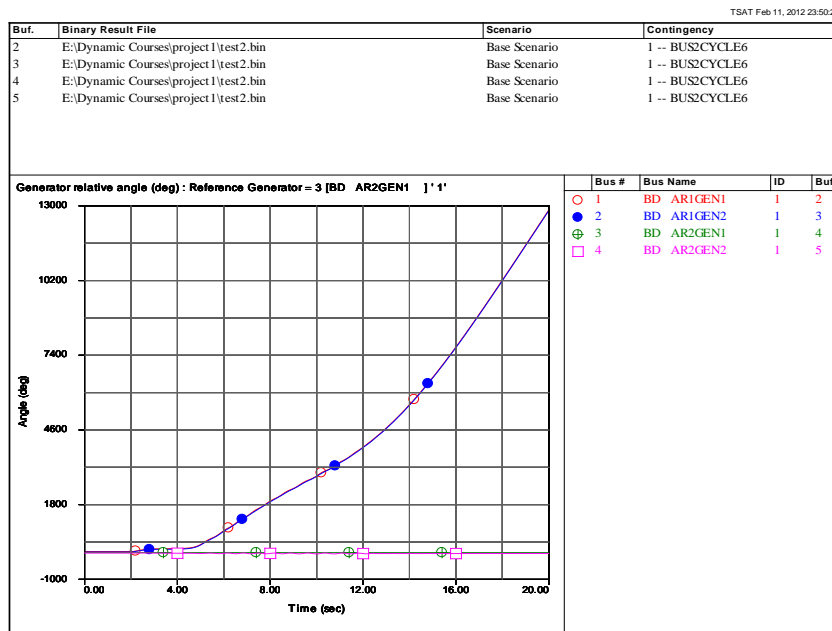
Generator phase angles when tie-line flow is 371MW (unstable)

- Fault at middle of lines between bus 2 and 5



DSATools Output Analysis 11.0
Powertech Labs Inc.
Copyright © 2012 All rights reserved

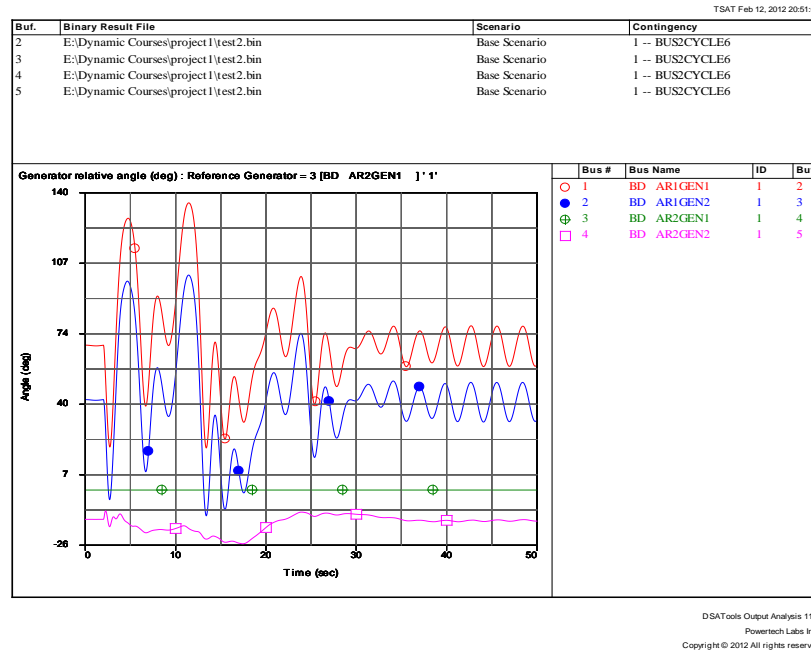
Generator phase angles when tie-line flow is 275 MW (stable)



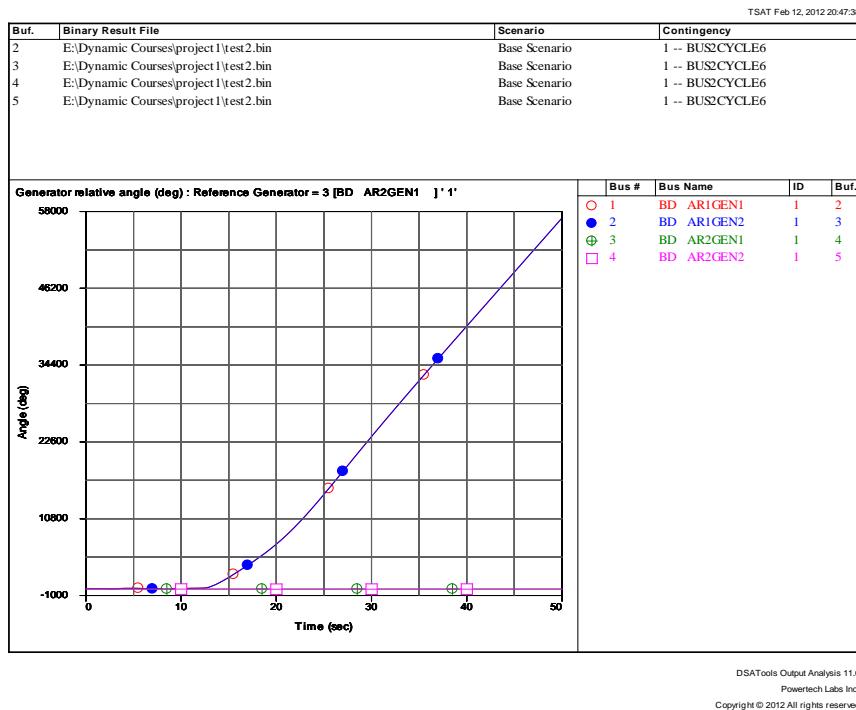
DSATools Output Analysis 11.0
Powertech Labs Inc.
Copyright © 2012 All rights reserved

Generator phase angles when tie-line flow is 276 MW (unstable)

- Fault at middle of lines between bus 4 and 6

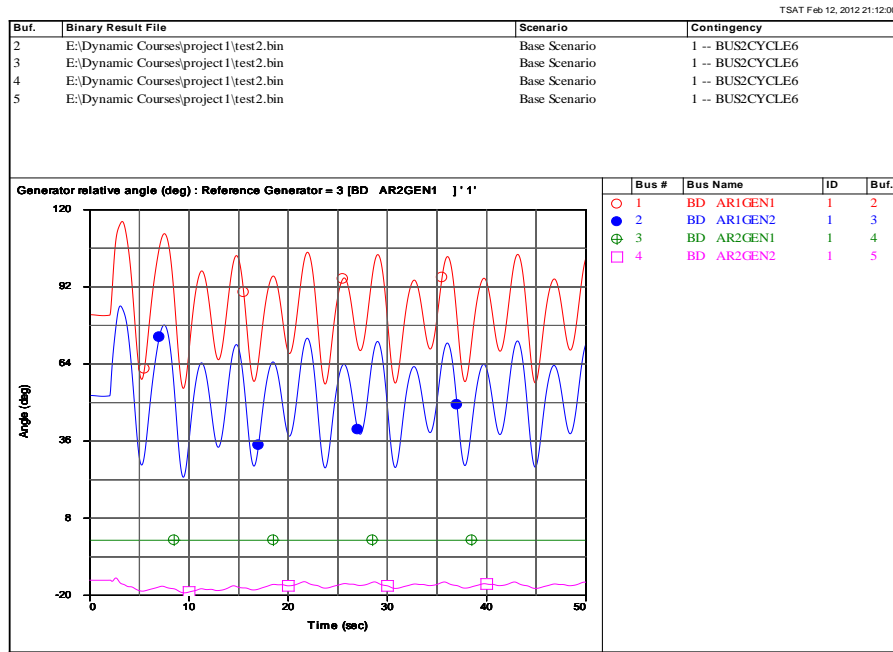


Generator phase angles when tie-line flow is 375 MW (stable)



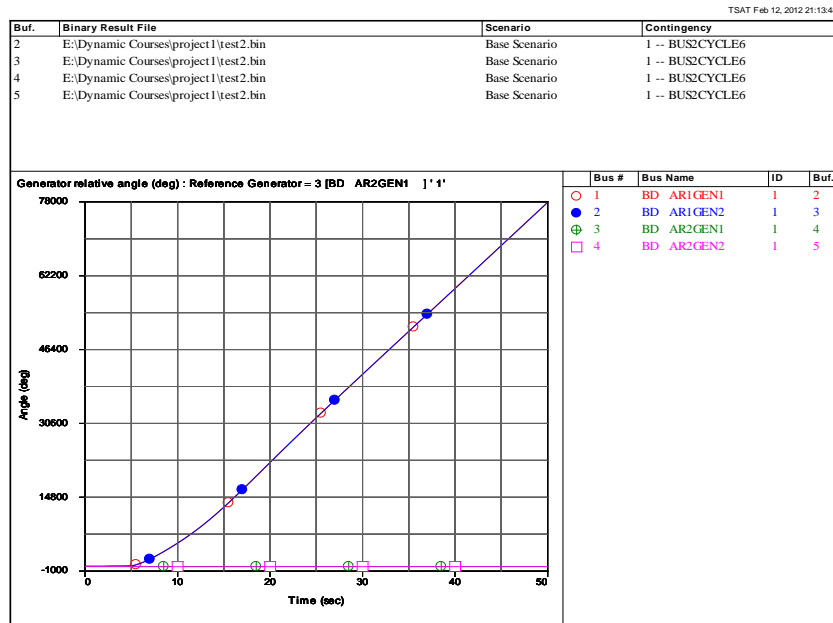
Generator phase angles when tie-line flow is 376 MW (stable)

- Fault at middle of lines between bus 5 and 6



DSATools Output Analysis 11.0
 Powertech Labs Inc.
 Copyright © 2012 All rights reserved

Generator phase angles when tie-line flow is 414 MW (stable)



DSATools Output Analysis 11.0
 Powertech Labs Inc.
 Copyright © 2012 All rights reserved

Generator phase angles when tie-line flow is 415 MW (unstable)

APPENDIX B

POWER FLOW DATA

0 100.0

100.0

1 'BD AR1' 230.00 2 0.000 0.000 1 1 1.03000 43.0363

2 'BD AR1' 230.00 2 0.000 0.000 1 1 1.01000 32.2011

3 'BD AR2' 230.00 3 0.000 0.000 2 2 1.03000 0.0000

4 'BD AR2' 230.00 2 0.000 0.000 2 2 1.01000 -9.7774

5 'B L' 230.00 1 0.000 223.500 1 1 0.98598 23.2790

6 'B L' 230.00 1 0.000 258.000 2 2 0.98660 -17.9830

0

5 BL 1 1 1 1241.000 100.000 0.000 0.000 0.000 0.000

6 BL 1 2 2 1699.000 100.000 0.000 0.000 0.000 0.000

0

1 1 790.00 77.59 500.00 -150.00 1.03000 0 100.00

2 1 790.00 277.09 500.00 -150.00 1.01000 0 100.00

3 1 713.80 71.46 500.00 -150.00 1.03000 0 100.00

4 1 740.00 243.37 500.00 -150.00 1.01000 0 100.00

0

1 2 1 0.00250 0.02500 0.00000 0.00 0.00 0.00 0.00000 0.00 0.00000

0.00000 0.00000 0.00000 1

2 5 1 0.00100 0.01000 0.00000 0.00 0.00 0.00 0.00000 0.00 0.00000

0.00000 0.00000 0.00000 1

5 6 1 0.02200 0.22000 0.00000 0.00 0.00 0.00 0.00000 0.00 0.00000

0.00000 0.00000 0.00000 1

3 4 1 0.00250 0.02500 0.00000 0.00 0.00 0.00 0.00000 0.00 0.00000
0.00000 0.00000 0.00000 1

4 6 1 0.00100 0.01000 0.00000 0.00 0.00 0.00 0.00000 0.00 0.00000
0.00000 0.00000 0.00000 1

0

0

1 1 600.000 3.000 'AREA1 '

2 3 -600.000 3.000 'AREA2 '

0

0

0

0

0

0

0 ' '

0 ' '

0 ' '

0 ' '

1 '1 '

2 '2 '

0

0

APPENDIX C
DYNAMIC DATA

DESC

CASE ID

TITLE - 1

TITLE - 2

TITLE - 3

TITLE - 4

TITLE - 5

TITLE - 6

EDATA

DGEN

1 1 100 100

0 0 30 0 0 0 0 0 0 0 0 0

0.00250 1.80000 1.70000 0.00000 .30000 .30000 0.0000 0.0000

8.00000 0.40000 .00000 .00000

6.50000 5.00000 .00000 900. 1.00 .00000

0 1 1 1

200.00000 .01000 1.00000 10.00000 .00000 0.0000 0.00000 .00000

5.00000 -5.0000 .00000 .00000 0.00000 0.0000 .00000 .00000

.01000 .00000 .00000 .00000 .00000 .00000 .00000 .00000

.00000 .00000 0.0 0.0

2 1 100 100

0 0 30 0 0 0 0 0 0 0 0 0

0.00250 1.80000 1.70000 0.00000 .30000 .30000 0.0000 0.0000

8.00000 0.40000 .00000 .00000
 6.50000 5.00000 .00000 900. 1.00 .00000
 0 1 1 1
 200.00000 .01000 1.00000 10.00000 .00000 0.0000 0.00000 .00000
 5.00000 -5.00000 .00000 .00000 0.00000 0.0000 .00000 .00000
 .01000 .00000 .00000 .00000 .00000 .00000 .00000 .00000
 .00000 .00000 0.0 0.0
 3 1 100 100
 0 0 30 0 0 0 0 0 0 0 0 0
 0.00250 1.80000 1.70000 0.00000 .30000 .30000 0.0000 0.0000
 8.00000 0.40000 .00000 .00000
 6.50000 5.00000 .00000 900. 1.00 .00000
 0 1 1 1
 200.00000 .01000 1.00000 10.00000 .00000 0.0000 0.00000 .00000
 5.00000 -5.00000 .00000 .00000 0.00000 0.0000 .00000 .00000
 .01000 .00000 .00000 .00000 .00000 .00000 .00000 .00000
 .00000 .00000 0.0 0.0
 4 1 100 100
 0 0 30 0 0 0 0 0 0 0 0 0
 0.00250 1.80000 1.70000 0.00000 .30000 .30000 0.0000 0.0000
 8.00000 0.40000 .00000 .00000
 6.50000 5.00000 .00000 900. 1.00 .00000
 0 1 1 1

```
200.00000 .01000 1.00000 10.00000 .00000 0.0000 0.00000 .00000
5.00000 -5.0000 .00000 .00000 0.00000 0.0000 .00000 .00000
.01000 .00000 .00000 .00000 .00000 .00000 .00000 .00000
.00000 .00000 0.0 0.0
```

EDATA

NLBS

```
5 0 0 0 0 0 0 0
```

```
6 0 0 0 0 0 0 0
```

EDATA

END